



Cite this: *Ind. Chem. Mater.*, 2024, 2, 191

## Design of functional binders for high-specific-energy lithium-ion batteries: from molecular structure to electrode properties

Tian Qin,<sup>†ab</sup> Haoyi Yang,<sup>†b</sup> Quan Li,<sup>\*b</sup> Xiqian Yu <sup>\*ab</sup> and Hong Li <sup>ab</sup>

The binder adheres to each component of the electrode to maintain the structural integrity and plays an irreplaceable role in a battery despite its low content. Polyvinylidene difluoride (PVDF), as the dominant binder in commercial battery systems (for cathodes), has acceptably balanced properties between chemical/electrochemical stability and adhesive ability. However, in the pursuit of high-specific-energy batteries featuring high mass loading, high voltage, and large volume changes, the PVDF binder is unable to satisfy the versatile electrode demands and extreme operation conditions. Therefore, developing novel binders with task-specific functionality is of urgent need. Herein, we review the recently developed design strategies of functional binders from the insight of molecular design. The functions and failure mechanisms of the binders are elucidated first. Starting from the basic moiety (functional group) of the polymer molecule, how the constituents, molecular structure, and assembly into a supramolecule will affect the properties of the binders, and furthermore the performance of the electrodes, is discussed at length. Finally, we summarize and provide a future outlook on the opportunities and challenges of functional binders towards future high-specific-energy lithium-ion batteries.

Received 16th August 2023,  
Accepted 28th September 2023

DOI: 10.1039/d3im00089c

rs.li/icm

Keywords: Functional binders; Molecular design; High-specific-energy electrodes; Lithium-ion batteries.

### 1 Introduction

The development of renewable energy technologies is imperative for sustainable development. However, the

intermittent nature of renewable energy necessitates the corresponding energy storage technology represented by rechargeable batteries. Renowned for their high energy density, high power density, and long life, lithium-ion batteries (LIBs) have been widely used in portable electronic devices, electric vehicles, and grid-scale energy storage systems.<sup>1–3</sup>

Increasing the energy density of LIBs remains a critical bottleneck for broadening the consumer market.<sup>4</sup> To date, significant efforts have been focused on the development of novel active electrode materials and electrolytes for both

<sup>a</sup> Center of Materials Science and Optoelectronics Engineering, University of Chinese Academy of Sciences, Beijing 100049, China. E-mail: xyu@iphy.ac.cn

<sup>b</sup> Beijing Frontier Research Center on Clean Energy, Huairou Division, Institute of Physics, Chinese Academy of Sciences, Beijing 100049, China

<sup>†</sup> These authors contributed equally to this work.



Tian Qin

Tian Qin is currently a graduate student at the Institute of Physics, Chinese Academy of Sciences (IOP, CAS). His research focuses on polymeric materials applied to lithium-ion batteries or lithium metal batteries.



Haoyi Yang

Haoyi Yang received his PhD degree in Materials Science and Engineering from Beijing Institute of Technology (BIT) in 2021. He is currently a postdoctoral fellow at the Institute of Physics, Chinese Academy of Sciences (IOP, CAS) and his research is focused on the electrode/electrolyte interface of lithium-ion batteries.



academic and market scenarios.<sup>5–7</sup> In contrast, the role of binders is much underestimated, and less effort has been devoted to improving battery performance *via* exploring and developing novel binders, compared to the rapid evolution of cathode and anode materials. Despite their small amount (~5 wt%) and inactivity, binders play a pivotal role in improving the electrochemical performance of batteries.<sup>8–13</sup>

There are many categories of binders, of which PVDF is the most widely used. PVDF ((CH<sub>2</sub>CF<sub>2</sub>)<sub>n</sub>) is a commonly used fluorinated plastic in daily life as coatings, binders, *etc.*, and the major large-scale fabrication methods of PVDF are emulsion or suspension polymerization with a vinylidene fluoride monomer, surfactant, and initiator.<sup>14</sup> Due to partial substitution of H atoms with F atoms in the vinylidene fluoride monomer compared with ethylene, PVDF possesses superior chemical, electrochemical, and thermal stability due to the higher bond energy of C–F bonds than C–H bonds.<sup>15</sup> The electrochemical window of PVDF is about 5 V and the thermal decomposition temperature is up to 400 °C.<sup>16</sup> Meanwhile, the presence of H is beneficial for the formation of hydrogen bonds (C–H···F or O–H···F). The interaction of PVDF with intermolecular polymer chains or adherent

surfaces by van der Waals forces and simultaneous hydrogen bonds can ensure the mechanical strength (30–70 MPa) of binders and adhesive strength. In stark contrast, completely F-substituted polytetrafluoroethylene (PTFE) exhibits weaker tensile strength (20–35 MPa) and adhesion due to the lack of intermolecular hydrogen bonds.<sup>17,18</sup> Moreover, PVDF has a swelling behavior (~30%)<sup>19</sup> and good crystallinity due to its linear molecular configuration. Thus, PVDF delivers good ionic conductivity after the uptake of electrolyte.<sup>20</sup> In short, PVDF shows appreciable comprehensive properties in practical aspects. That is why, when employed as a binder in LIBs, PVDF exhibits well-balanced performance, and it has become the most dominant binder (usually in cathodes). The annual demand for battery-grade PVDF has reached the level of ten thousand tons in China, which has also brought about a rapid rise in PVDF prices.

Despite its successful application in conventional battery systems, such as lithium cobalt oxides (LiCoO<sub>2</sub>, LCO) (<4.6 V) or lithium iron phosphate (LiFePO<sub>4</sub>, LFP)/graphite, PVDF has not perfectly satisfied the requirements for utilization in high-specific-energy electrode materials in next-generation battery systems, *e.g.*, Ni-rich layered oxide cathodes (LiNi<sub>x</sub>Co<sub>y</sub>Mn<sub>z</sub>O<sub>2</sub> ( $x + y + z = 1$ ), NCM<sub>xyz</sub>),<sup>19,21</sup> high-voltage LCO (≥4.6 V),<sup>22</sup> Li-rich Mn-based oxide (xLi<sub>2</sub>MnO<sub>3</sub>·(1-x)LiMO<sub>2</sub> (M = Mn, Ni, Co),<sup>23,24</sup> LRMO) cathodes, spinel oxide (LiMn<sub>2</sub>O<sub>4</sub>, LMO; and LiNi<sub>0.5</sub>Mn<sub>1.5</sub>O<sub>4</sub>, LNMO) cathodes,<sup>25</sup> silicon anodes,<sup>26–30</sup> silicon oxide anodes<sup>31,32</sup> and lithium metal anodes.<sup>33–35</sup> There are some pivotal challenges in next-generation electrode materials that PVDF does not satisfactorily cover: (1) ultra-high mass loading. It is a feasible and effective way to increase the battery energy density by increasing the electrode areal mass loading,<sup>36,37</sup> but with the increase of the loading, higher requirements are put forward for the adhesive strength of the binder to maintain the integrity of the electrode.<sup>38–41</sup> However, the electron cloud density and the polarizability of PVDF are low, so the interaction between PVDF and other molecules through van der Waals forces is relatively weak, which is insufficient for ultra-high mass loading electrodes (>20 mg cm<sup>-2</sup>);<sup>17,18</sup> (2) large volume variations. This is the most



Quan Li

*Quan Li is currently a postdoc at the Institute of Physics, Chinese Academy of Sciences. His recent research mainly focuses on high energy density lithium batteries, lithium metal batteries and electrode interfaces.*



Xiqian Yu

*Xiqian Yu is currently a professor at the Institute of Physics, Chinese Academy of Sciences (IOP, CAS). His research interest is in the field of electrochemical energy storage with the main focus on the characterization of electrode materials for rechargeable batteries.*



Hong Li

*Hong Li is a professor at the Institute of Physics, Chinese Academy of Science (IOP, CAS). His research interests include fundamental research in batteries, such as the transport of ions and electrons, size effects, interface phenomena, structure evolution as well as application research, including high energy density Li-ion batteries using a Si-based anode, solid lithium batteries and their failure analysis.*



common and intractable problem in many high-capacity cathodes and especially in anode materials, such as LCO (−11.7%)<sup>42</sup> and Si (more than 300%).<sup>29</sup> For silicon anodes, repeated volume changes easily lead to the loss of the contact between particles and conductive additives, as well as between the electrodes and the current collector. In addition, iterative volume changes over the cycles break the solid electrolyte interphase (SEI) and expose the electrode surface to the electrolyte, which re-generates the new SEI and consumes the electrolyte. In addition, the mechanical stresses originating from the volume changes can cause particle pulverization, which results in detachment of particles from the electrode surface.<sup>9</sup> However, PVDF is difficult to adapt to large volume changes due to a weak adhesive force and poor mechanical properties. The large volume changes result in binder failures, such as binder debonding, polymer plastic deformation, and even fracture.<sup>43,44</sup>

In addition to the basic need of adhesion, some specific functions can also be realized *via* functional binders to boost the batteries' electrochemical performances significantly, although it is commonly considered that other electrode components, such as electrolytes and additives, are primarily required to realise these functions. These unique functions that PVDF does not possess are afforded by the binder molecule design and are as follows. (1) Mitigating interface degradation: a variety of high-voltage cathodes, such as LCO, NCM, LMO, LRMO, *etc.*, will release oxygen at high voltage, of which the aftermaths are surface lattice reconstruction and transition-metal dissolution into the electrolyte.<sup>45–48</sup> Meanwhile, other active species from the electrolyte, such as free radicals and HF, can attack the cathode and anode surfaces and accelerate this process.<sup>49,50</sup> The by-products built up on the surface are recognized to result in an unstable cathode electrolyte interphase (CEI) and SEI. These effects will reduce the structural stability and impede the electrode dynamics, further degrading the battery performance. Concerning this problem, PVDF does not protect the electrode interface well enough. Owing to the low electron density of C–F bonding, PVDF is also unable to capture various active intermediates and thus it is difficult to inhibit the interface degradation.<sup>51</sup> (2) Providing electronic or ionic conductivity: due to the poor electric and ionic conductivity of most active materials, additional conductive materials, such as conductive carbons or electrolytes, are required in the electrodes, which reduces the overall energy density of the batteries. Although PVDF can permit ion diffusion after swelling, it does not conduct electrons, which also hinders charge transfer and affects battery rate performance.<sup>20</sup> (3) Improving thermal stability: As the energy density increases, the thermal safety of the new electrode system generally decreases.<sup>52,53</sup> Novel high-specific-energy electrode materials may pose potential thermal safety risks, but this has not been explored in great detail.<sup>54</sup> Owing to the large amount of electrolyte absorbed by PVDF, the thermal safety of batteries can be compromised.<sup>55</sup> (4) Homogeneous dispersion of the electrode components: particles are prone

to self-agglomeration as the size decreases, such as Si nanoparticles.<sup>56</sup> The interaction of PVDF with the hydrophilic surface of the active materials is weak (owing to the low polarity of C–F bonding) and it is thus difficult to promote uniform dispersion of the electrodes.<sup>19</sup> (5) High compatibility with new manufacturing: for example, in the preparation of sulfide-based all-solid-state batteries, the solution-based processing requires the use of a weakly polar solvent to avoid the reaction of the strong polar solvent with the sulfide electrolyte, but low-polarity solvents cannot easily dissolve conventional polar binders such as PVDF.<sup>57</sup> Because of the incompatibility of PVDF with the wet-slurry manufacturing of sulfide solid electrolytes, new binders suitable for solid-state electrolyte manufacturing need to be developed.<sup>58</sup> In addition, the chemical and electrochemical compatibilities of binders with other electrode components also need to be considered carefully. It is believed that, because there is partial substitution of hydrogen atoms by fluorine atoms in PVDF, the strong electron-withdrawing inductive effect of the fluorine atoms leads to strong acidity of the hydrogen on the  $\beta$ -carbon, which easily undergoes an alkali- or nucleophile-induced E2 elimination reaction to eliminate HF.<sup>59</sup> The generated HF and water cause serious damage to the electrode interface, as demonstrated by previous reports in the literature.<sup>60</sup> In addition, the double bonds generated by the E2 elimination are prone to cross-linking with other PVDF molecules to increase the viscosity of the slurry, resulting in poor fluidity and uneven coatings.<sup>61</sup> The base usually comes from the residual base on the cathodes and NMP solvent. Especially with high-nickel cathodes, the gel phenomenon of the slurry is more intractable. In addition to upgrading the manufacturing process or neutralizing the basic environment, the alkali resistance of the binder needs to be considered when designing the binders. Anyhow, it should be noted that the prior and basic concern for a binder is always the adhesion.

Therefore, it is of great importance to develop new functional binders with careful design. We are expected to deal with the following challenges for high-specific-energy electrodes: (1) high mass loading; (2) large volume change; (3) high voltage; (4) low rate performance; (5) potential thermal risk; and (6) the compatibility of new manufacturing (*e.g.*, preparation of solvent-free electrodes or sulfide-based all solid-state batteries). The binders are expected to possess the following characteristics: (1) high adhesive and mechanical strength; (2) high elasticity or self-healing ability; (3) the ability to mitigate interphase degradation; (4) high electric and ionic conductivity; (5) the ability to improve thermal safety and wide-temperature operability; and (6) the ability to promote the heterogeneous dispersion of each component.

Rational molecular design is highly effective when developing new binders for improved battery performance.<sup>62,63</sup> From the view of the molecular structure, the binder is a polymer material with multiple molecular moieties and corresponding properties from micro- to macro-views, such as molecular weight and molecular weight



distribution, functional groups and topologic molecular configurations (linear, branched, hyperbranched and network cross-linking). The interaction forces can hence be designed in binder molecules based on the molecular structure, which includes molecular bonding and intermolecular bonding (also known as supramolecular interactions).<sup>10</sup> Molecular bonds are mainly covalent bonds between polymeric units. Intermolecular forces are typified by van der Waals forces and secondary bond forces (hydrogen bonds, ion-ion, dipole-dipole,  $\pi$ - $\pi$  interactions, coordination and hydrophobic interactions). Hydrophobic interactions should be avoided because they induce binder agglomeration. To obtain the functional binders, common modification and synthesis methods for functional polymers include grafting,<sup>64</sup> copolymerization,<sup>65</sup> cross-linking,<sup>66</sup> and blending.<sup>51</sup> Well-designed polymers with different molecular structures and interaction forces have been applied to achieve customized and functional modifications to improve the task-specific performance of high-specific-energy electrodes.

Common binders used in electrodes include PVDF, PTFE, poly(acrylic acid) (PAA), styrene-butadiene rubber (SBR), polyethylene oxide (PEO), sodium carboxymethylcellulose (CMC), and alginate. The elementary properties of these binders, including tensile and compressive mechanical properties, adhesive force, and thermal properties are summarized in Tables 1, 2, 3 and 4, respectively. Among them, the tensile parameters, including elastic modulus, yield elongation, yield strength, ultimate strength, and break elongation, indicate the resistance for the volume expansion of the electrodes, while the compressive parameters, including reduced modulus, and hardness, present the strength of the electrodes to maintain the structural integrity

when pressure is applied. Based on this endeavour, we are able to compare these seven common binders in terms of adhesion, tensile strength, elasticity, swelling, ionic conductivity, thermal stability, and oxidation stability, as shown in Fig. 1. It is worth noting that the comparison is semi-quantitative because the collected data is from different papers under different experimental methods and conditions. PVDF still has a better comprehensive performance than other binders.<sup>16</sup> The fully fluorinated form, PTFE, has extremely unbalanced performance, whereby its mechanical properties and oxidation stability are the best, while the adhesion and conductivity are inferior. PAA, CMC and alginate, widely used in anodes, appear inferior in terms of mechanical properties than PVDF, but they are water-soluble and rich in carboxyl or hydroxy groups contributing to stronger adhesion.<sup>67-69</sup> SBR has very high elasticity and is usually blended with CMC to complement each other's disadvantages.<sup>70</sup> It is well-known that PEO has an outstanding ionic conductivity but inferior resistance to oxidation under high voltage.<sup>71</sup>

Herein, in this review, we firstly aim to present the effect of molecular structure on the properties of the binders and on the macroscopic electrochemical properties of the electrode. We highlight the versatile influences of the binders on the mechanical, interfacial, electrical, thermal and dispersive properties of the electrodes. The fruitful efforts in binder molecule design are summarized according to the functionality of the binders, and in each section we will present the function/failure mechanics of the binders and the corresponding molecular design strategies. We hope to provide insight into the function of binders in various high-specific-energy electrode materials,

**Table 1** The tensile mechanical properties of binders

| Category             | Binders           | Characteristic functional groups          | Elastic modulus (MPa) | Yield elongation (%) | Break elongation (%) | Yield strength (MPa) | Ultimate strength (MPa) | Reference             |
|----------------------|-------------------|---|-----------------------|----------------------|----------------------|----------------------|-------------------------|-----------------------|
| Alkane-based         | PVDF              | Fluorine                                  | 1400                  | 30                   | 30                   | 40                   | 40                      | 16, 32, 43, 44, 72-77 |
|                      | PTFE              | Fluorine                                  | 400-1800              | —                    | 50-650               | 9-30                 | 10-43                   | 78                    |
|                      | PAA               | Carboxyl                                  | 450                   | <5                   | <5                   | <10                  | <10                     | 30, 32, 79, 80        |
|                      | PEO               | Ether                                     | 700                   | —                    | <10                  | —                    | 15                      | 16, 32, 74            |
|                      | SBR               | Alkene, phenyl                            | 1.31                  | —                    | 385                  | —                    | 3.33                    | 70                    |
|                      | PAA-P(HEA-co-DMA) | Hydroxy, carboxyl, catechol               | 1.6                   | ~50                  | >400                 | 0.8                  | 1.2                     | 30                    |
|                      | SHP               | Ureido                                    | >3.6                  | 75                   | 300                  | 0.9                  | 1                       | 81                    |
|                      | Anti-aging binder | Amino                                     | 60                    | 120                  | 280                  | 70                   | 70                      | 72                    |
|                      | N-P-LiPN          | Ionized fragment, carboxyl, sulfonic acid | ~80                   | 8                    | >30                  | 4                    | 4                       | 28                    |
|                      | DPGP-PEI/PVDF     | Amino, catechol, ether, pentafluorophenol | ~800                  | 5                    | 70                   | 40                   | 40                      | 51                    |
| Polysaccharide-based | PEO-polycarbonate | Ether, phosphate group, ester             | 0.33                  | >1000                | >1000                | >3.5                 | >3.5                    | 65                    |
|                      | PR-PAA            | Carboxyl, hydroxyl, urethane, ether       | 2                     | 50                   | 400                  | 1                    | 1.6                     | 26                    |
|                      | CMC               | Carboxyl, hydroxy                         | 1400                  | —                    | <10                  | —                    | 40                      | 69, 79, 82            |
|                      | Alginate          | Carboxyl                                  | 1400                  | —                    | 15                   | —                    | 30                      | 73, 82, 83            |
| Inorganic            | CMC-CNT           | Carboxyl, hydroxy                         | 1000                  | ~2                   | ~2                   | 20                   | 20                      | 84                    |
|                      | UCFR              | Ionized fragment                          | 60                    | 5                    | 6                    | 3                    | 3                       | 85                    |





**Table 2** The compressive mechanical properties of binders

| Category     | Binders              | Characteristic functional groups                | Reduced modulus (MPa)            | Hardness (MPa) | Reference             |
|--------------|----------------------|---|----------------------------------|----------------|-----------------------|
| Alkane-based | PVDF                 | Fluorine  | 600–4000                         | 25–200         | 16, 32, 43, 44, 72–77 |
|              | PAA                  | Carboxyl  | ~8000                            | ~200           | 30, 32, 79, 80        |
|              | PEO                  | Ether   | 500–1000                         | 70–82          | 16, 32, 74            |
|              | SBR                  | Alkene, phenyl                                  | 5.57                             | 0.27           | 86                    |
|              | HOS-PFM              | Fluorene, carbonyl, ester                       | ~9000                            | ~200           | 32                    |
|              | N-P-LiPN             | Ionized fragment, carboxyl, sulfonic acid group | 900                              | 20             | 28                    |
|              | Mn-COP               | Mn <sup>2+</sup> -Loporphyrin, thioureido       | —                                | 70             | 44                    |
|              | 3F1V                 | Hydroxyl, ether                                 | 1500                             | 50             | 87                    |
|              | Polysaccharide-based | XG  | Hydroxy, ester, ionized fragment | 1000           | 25                    |
| GG           |                      | Hydroxyl  | 1500                             | 24             | 66, 75                |
| TG           |                      | Carboxyl, hydroxyl                              | 3500                             | 324            | 74                    |
| N-GG-XG      |                      | Hydroxyl, ionized fragment                      | 1500                             | 30             | 66                    |
| Gelatin      |                      | Hydroxyl  | 1800                             | 25             | 66                    |
| GG-g-PAM     |                      | Hydroxyl, amide                                 | 2100                             | 60             | 75                    |

**Table 3** The adhesive forces of binders

| Category             | Binders           | Characteristic functional groups          | Adhesion force (N cm <sup>-1</sup> ) | Reference             |
|----------------------|-------------------|---|--------------------------------------|-----------------------|
| Alkane-based         | PVDF              | Fluorine                                  | ~1                                   | 16, 32, 43, 44, 72–77 |
|                      | PAA               | Carboxyl                                  | 1.5                                  | 30, 32, 79, 80        |
|                      | PEO               | Ether                                     | <0.5                                 | 88, 89                |
|                      | SBR               | Alkene, phenyl                            | 0.1–0.5                              | 90, 91                |
|                      | C10               | Phenyl, carboxyl                          | 0.05                                 | 58                    |
|                      | Anti-aging binder | Amino                                     | 8.9                                  | 72                    |
|                      | DPGP-PEI/PVDF     | Amino, catechol, ether, pentafluorophenol | 0.67                                 | 51                    |
|                      | PEO-polycarbonate | Ether, phosphate group, ester             | 6                                    | 65                    |
|                      | Spandex           | Ether, urethane, ureido                   | 1.66                                 | 43                    |
| Polysaccharide-based | CMC               | Carboxyl ion                              | 1.1–1.7                              | 69, 79, 82            |
|                      | Alginate          | Carboxyl ion                              | 2                                    | 73, 82, 83            |
| Inorganic            | APP               | Phosphate                                 | 0.3                                  | 92                    |

**Table 4** The thermal properties of binders

| Category     | Binders              | Characteristic functional groups            | T <sub>g</sub> (°C) | T <sub>d</sub> (°C) | Reference             |            |
|--------------|----------------------|---|---------------------|---------------------|-----------------------|------------|
| Alkane-based | PVDF                 | Fluorine                                    | -38                 | 400                 | 16, 32, 43, 44, 72–77 |            |
|              | PTFE                 | Fluorine                                    | -103                | 400                 | 78                    |            |
|              | PAA                  | Carboxyl                                    | 115                 | 150                 | 30, 32, 79, 80        |            |
|              | PEO                  | Ether                                       | -50                 | 350                 | 16, 32, 74            |            |
|              | SBR                  | Alkene, phenyl                              | -60                 | 400                 | 93                    |            |
|              | HOS-PFM              | Fluorene, carbonyl, ester                   | —                   | >800                | 32                    |            |
|              | PAA-P(HEA-co-DMA)    | Hydroxy, carboxyl, catechol                 | 83                  | —                   | 30                    |            |
|              | PEO-polycarbonate    | Ether, phosphate group, ester               | -40                 | 200                 | 65                    |            |
|              | c-PEO-PEDOT:         | Amino, ether, sulfonic acid group, ethylene | —                   | >200                | 94                    |            |
|              | PSS/PEI              | dioxythiophene                              | —                   | —                   | —                     |            |
|              | PVDF-TrFE-g-SPS      | Fluorine, sulfonic acid group               | 100                 | 400                 | 95                    |            |
|              | Spandex              | Ether, urethane, ureido                     | —                   | 300                 | 43                    |            |
|              | (Deprotect) TBA-b-BR | Carboxyl                                    | 210                 | 400                 | 96                    |            |
|              | Polysaccharide-based | CMC   | Carboxyl ion        | 55                  | 300                   | 69, 79, 82 |
|              |                      | Alginate                                    | Carboxyl ion        | 119                 | 200–500               | 73, 82, 83 |
| TG           |                      | Carboxyl, hydroxyl                          | —                   | 250                 | 74                    |            |

especially for the ones that suffer from large volume changes, mechanical fracture, reactive interfaces or even poor conductivity. Finally, we provide a future perspective on the research of binders with regard to advanced characterization methods and simulations for the next generation of high-specific-energy electrodes.

## 2 Functionality of binders in LIBs

### 2.1 Mechanical properties

#### 2.1.1 Improvement of adhesion and mechanical strength.

Keeping an effective contact between the active materials, conductive carbons and current collector, and maintaining



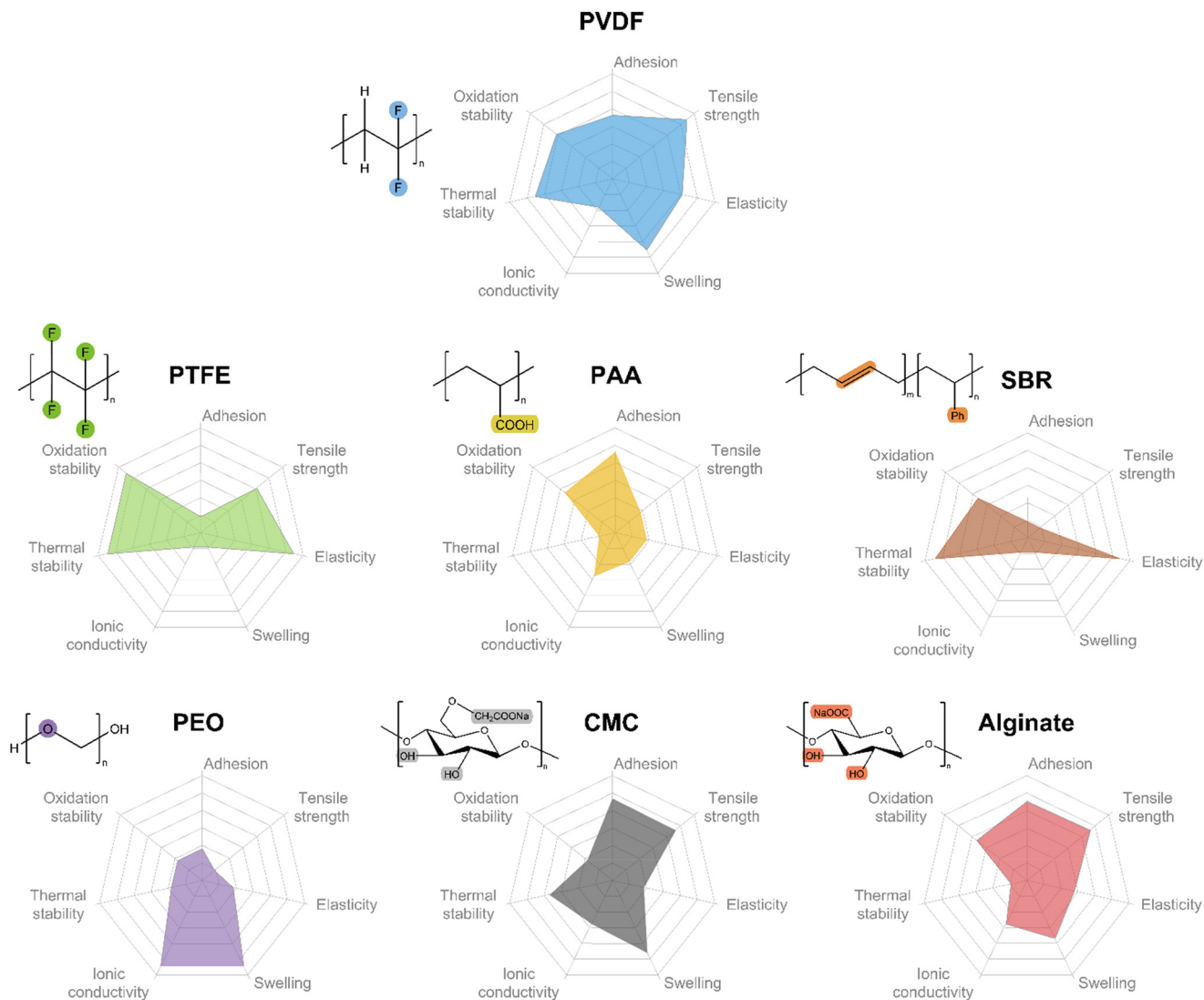


Fig. 1 Comparison of the basic properties of common binders, *i.e.*, PVDF, PTFE, PAA, SBR, PEO, CMC, and alginate.

the integrity of the electrode are the most fundamental and important functions of binders. Conversely, binding failure refers to the loss of adhesive force, which leads to the detachment of electrodes from current collectors and the delamination of active materials from electrode surfaces. This structural destruction contributes to the disruption of ion and electron pathways and the loss of active materials, which is closely associated with the capacity decay. Therefore, the binder adhesion is of great importance to normal battery operation.<sup>97,98</sup> The adhesion failure mechanisms can be typically summarized as being due to three reasons: contact interface destruction, binder rupture and adherend breakage (Fig. 2a). Interface destruction means adhesive force disappearance and a loss of contact between the binders and adherend. Binder rupture refers to the breakdown of molecular adhesion, and adherend breakage means the rupture of the adherend (*i.e.*, electrode). Upon increasing the mass loading of electrodes for high-specific-energy batteries, stronger adhesion is required to attach to more active

materials and maintain the structural stability.<sup>89,99</sup> However, the commonly used binder PVDF cannot ideally cover the aforementioned need. The C–F bonds in PVDF interact with adherends *via* weak van der Waals forces and the adhesion is insufficient to maintain the electrode integrity when the loading is extremely high. At the same time, PVDF readily absorbs electrolyte, *i.e.*, swelling, which weakens the adhesion and mechanical strength of the binders and leads to potential instability of electrode integrity.

Targeted at the failure mechanism, the corresponding solutions for adhesion failure and binder rupture are the improvement of interfacial adhesion and binder cohesion. From the perspective of molecular design, adhesion can be enhanced by introducing functional groups with stronger interactions with interfaces, such as hydrogen bonds,<sup>29</sup> coulombic attraction<sup>38,85</sup> and  $\pi$ - $\pi$  stacking,<sup>31,100</sup> in place of van der Waals forces. Inspired by mussels, which can adhere on stones in water tightly, catechol, abundant in the byssus of mussels, was demonstrated to have a powerful adhesion



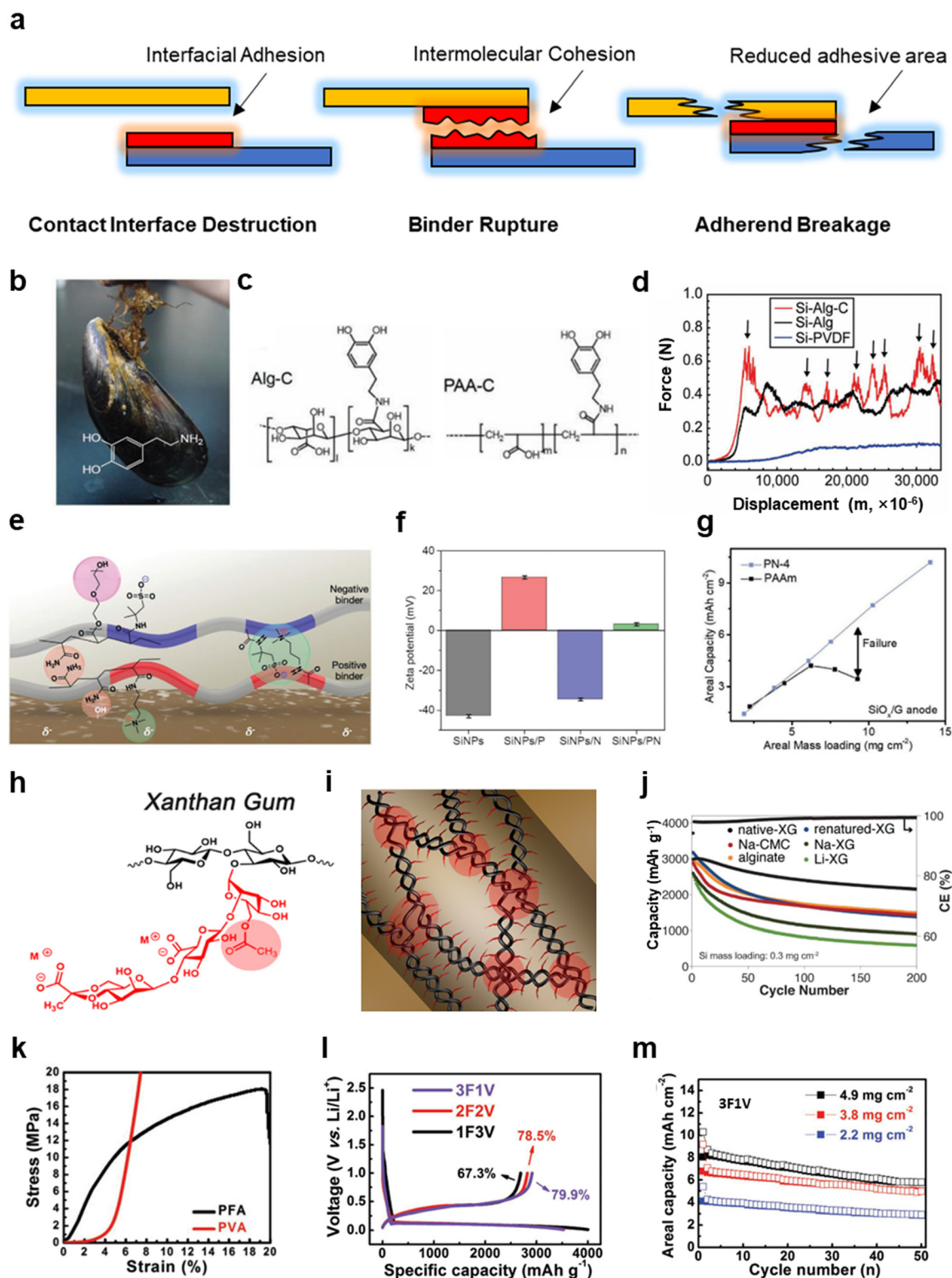


**Fig. 2** Modification strategies to improve the adhesion and mechanical strength of functional binders. (a) Typical adhesion failure mechanisms of binders. (b) Optical image of a mussel and the chemical structure of dopamine (inset). (c) Molecular structures of catechol-grafted alginate (Alg-C) and PAA (PAA-C). (d) Peeling-off test for Si electrodes with alginate-based binders and PVDF. (b)–(d) are reproduced with permission.<sup>29</sup> Copyright 2013, Wiley. (e) Schematic illustration of the interaction between charged binders. (f) Zeta potential of Si and Si with the charged binders. (g) The relationship of the delivered areal capacity and mass loading of a SiO<sub>x</sub>/graphite anode. (e)–(g) are reproduced with permission.<sup>38</sup> Copyright 2023, Wiley. (h) Chemical structure of xanthan gum (XG). (i) Schematic illustration of double helical structure and multiple short chains of XG. (j) Cycling performance of Si electrodes with XG-based binders, CMC and alginate at 1 C. (h)–(j) are reproduced with permission.<sup>82</sup> Copyright 2015, Royal Society of Chemistry. (k) Tensile test of PFA and PVA films. (l) Initial charge/discharge profiles for Si electrode with 3F1V, 2F2V and 1F3V; (m) cycling performance of the Si electrode using 3F1V at different loadings. (k)–(m) are reproduced with permission.<sup>87</sup> Copyright 2019, Wiley.



structure due to strong interaction between the hydroxyl groups and a hydrophilic surface, such as a Si surface (Fig. 2b).<sup>29</sup> The catechol structures were grafted onto PAA and sodium alginate as PAA-C and alginate-C (Fig. 2c). Peeling-off tests indicated that the Si anodes with alginate-C binders exhibited stronger adhesive forces than the alginate- and PVDF-based Si anodes (Fig. 2d). Alginate-C/Si and alginate/Si in half-cell tests exhibited capacities of more than 2000 mA h g<sup>-1</sup> and 1500 mA h g<sup>-1</sup>, respectively, both with an average coulombic efficiency exceeding 99% after 400 cycles. This strategy of grafting catechol structures onto binder molecules has also been validated by many other works that report enhanced adhesion.<sup>51,101–103</sup> Coulombic attraction is also a powerful option to enhance the adhesion of binders. Han *et al.* designed two kinds of copolymer binders with a positive and negative charge, respectively, derived from a quaternary ammonium salt and a sulfonate.<sup>38</sup> The coulombic interactions between positive and negative binders, and between positive binders with a negatively charged surface of Si particles, guarantees the cohesion within binders and the integrity of the particle–binder surface, as shown in Fig. 2e. Zeta potential tests proved the positively or negatively charged properties of Si particles, Si/positive binders, Si/negative binders and Si/positive binders/negative binders (Fig. 2f). As mentioned above, the tight adhesion is beneficial to high mass loading. The capacity is evidently reduced when the areal mass loading of SiO<sub>x</sub>/graphite anodes with poly(acrylamide) as binders exceeded 6 mg cm<sup>-2</sup>. In contrast, ultra-high-loading electrodes could be fabricated with the charged binders. The mixture mass loading reached 14 mg cm<sup>-2</sup> and the areal capacity reached 10.2 mA h cm<sup>-2</sup> without capacity loss (Fig. 2g).

Binder molecular strength can be increased by cross-linking, which can be divided into physical cross-linking and chemical cross-linking. Physical cross-linking indicates there are strong intermolecular interactions without chemical bonding, such as double-helix structures.<sup>66,82,104</sup> For example, the Choi group used xanthan gum (XG) as a binder. The structural formula is shown in Fig. 2h.<sup>82</sup> Attributed to the hydrogen bonding attraction of the saccharide backbone and the electrostatic repulsion of the side chains, XG was wrapped in a double helix, which immensely enhanced its molecular mechanical strength (Fig. 2i). Meanwhile, analogous to millipedes' pads, the side chains interacted with the silicon surface *via* large quantities of noncovalent interactions, such as hydrogen bonds and ion-dipole interactions, further enhancing the adhesion. Compared to various polysaccharide binders, native-XG exhibited excellent cycling performance (Fig. 2j). The capacity retentions of Si/native-XG, Si/alginate and Si/CMC (typically CMC refers to Na-CMC unless otherwise stated) were 72.2%, 50.3% and 49.7% after 200 cycles, respectively. It should be noted that Si/renatured-XG provided a far inferior capacity retention, either because the double-helix structures were damaged under heating conditions, or due to possible agglomeration. Chemical cross-links entail the formation of intermolecular chemical bonds, which significantly enhance the strength of the binder

networks compared with physical cross-links.<sup>105,106</sup> For instance, the hydroxyl groups of CMC and the carboxylic groups of PAA can initialize a condensation reaction under vacuum conditions at 150 °C, and the product demonstrated improved molecule rigidity allowing it to better adapt to the large volume change.<sup>56</sup> Assisted by ionic cross-linking agents, Wu *et al.* utilized Mn<sup>2+</sup>, Al<sup>3+</sup>, Ba<sup>2+</sup>, Na<sup>+</sup>, Ca<sup>2+</sup> and Zn<sup>2+</sup> to cross-link alginate, among which Al<sup>3+</sup>-alginate and Ba<sup>2+</sup>-alginate have the most obvious effect on the improvement of viscosity and hardness in a Si electrode.<sup>107</sup> Moreover, Li *et al.* utilized epichlorohydrin (ECH) to cross-link peach gum (PG), named as PG-*c*-ECH, for use as Si anode binders.<sup>108</sup> Nanoindentation tests demonstrated that Si@PG-*c*-ECH had larger modules and hardness. The Si@PG-*c*-ECH electrodes exhibited a discharge capacity of 2060 mA h g<sup>-1</sup> after 200 cycles and a capacity retention of 88.8% (based on the second cycle). In contrast, Si@sodium alginate and Si@PG have only 40.4% and 66.5% capacity retention, respectively.

Apart from electrodes, binders can also be utilized for solid-state electrolytes. Cao *et al.* used ethyl cellulose as a binder in a sulfide-based electrolyte (Li<sub>6</sub>PS<sub>5</sub>Cl).<sup>109</sup> Benefitting from the adhesion of the binder, the electrolyte exhibited superior mechanical strength and integrity. Thinner and more rigid electrodes can be prepared. The thickness of the sulfide electrolyte was 47 μm and there was no fracturing, even at 80 MPa compression stress. As the thickness and mass of the electrolyte decreases, the energy density of the battery can be increased. Using a cell comprising a LCO/Li<sub>2</sub>-InCl<sub>6</sub> cathode (55 μm), Li<sub>6</sub>PS<sub>5</sub>Cl electrolyte (50 μm) and Li-In anode (30 μm), the all-solid-state battery delivered 175 W h kg<sup>-1</sup> gravimetric energy density and 670 W h L<sup>-1</sup> volumetric energy density.

An ingenious strategy can improve both adhesion and strength simultaneously, that is, the combination of rigid and flexible chains in polymeric binders. Rigid chains provide strength, while soft chains provide adhesion. Poly(furfuryl alcohol) (PFA) has a high Young's modulus and high ultimate strength, while polyvinyl alcohol (PVA) has a large ultimate elongation and low ultimate strength (Fig. 2k). Therefore, combining soft PFA and rigid PVA *via* an *in situ* polymerization, Lu's group constructed a 3D interpenetrating binding network for Si anodes.<sup>87</sup> Different ratios of PFA and PVA were utilized including 75:25, 50:50 and 25:75, denoted as 3F1V, 2F2V and 1F3V, respectively. Initial charge specific capacities of the Si anodes with 1F3V, 2F2V and 3F1V binders were 2692.6, 2822.3, and 2916.5 mA h g<sup>-1</sup>, corresponding to coulombic efficiencies of 67.3%, 78.5%, and 79.9%, respectively (Fig. 2l). 3F1V with superior capacity fulfillment also showed good cycling performance for Si electrodes, even at a high mass loading of 4.9 mg cm<sup>-2</sup> (Fig. 2m). Full batteries were assembled using LRMO cathodes and Si anodes, and they delivered an areal capacity of >10 mA h cm<sup>-2</sup> and an energy density of >300 W h kg<sup>-1</sup>.

**2.1.2 Volume change accommodation.** Many high-specific-energy electrodes are inevitably confronted with severe volume changes upon large amounts of Li uptake/release





during charge and discharge, such as high-voltage oxide cathodes (LCO (11.7%),  $\text{Li}_2\text{MnO}_3$  (40.8%)),<sup>42</sup> alloy anodes (silicon anodes (~300%)), conversion electrodes (sulfur cathodes (~80%), metal oxides (20–100%), metal fluorides (10–40%), metal sulfides (40–170%)),<sup>110,111</sup> and even lithium metal anodes. The problems induced by volume change are schematically illustrated in Fig. 3a. The repeated volume fluctuation induces poor contact between the active material particles and inactive functional components in the electrode matrix. Delamination is induced as the electrode particles undergo as little as 7.5% volume change according to the theoretical prediction.<sup>112</sup> This issue actually impairs the structural integrity and disrupts the charge transport pathways. Furthermore, vulnerable electrode–electrolyte interfaces cannot endure severe volume changes, and are easy to break. In addition, the exposed surface of the active materials will consume extra electrolyte and Li ions as well as regenerate thicker interfaces, causing capacity losses and a large interfacial impedance. Moreover, the stress/strain resulting from huge volume changes intensifies the particle pulverization, especially for microparticle silicon (SiMP) compared to nanoparticle silicon (SiNP), leading to the exposure of more surface to the electrolyte. Also, dispersed particles lose the pathways to transfer electrons and ions. Some strategies are proposed to ameliorate the negative effects from volume change, such as a special yolk–shell structure<sup>113</sup> and an elastic binder.<sup>30</sup> Although binders are believed to be an ideal volume buffer inside the electrode matrix, the binder itself suffers from mechanical failure. The stress–strain curve of polymers is shown schematically in Fig. 3b. When the stress arising from volume changes is within the elastic limit of the polymers, the polymers' deformation belongs to elastic deformation, which means that the polymers can recover when the stress is removed. Therefore, as we expected, the binders can endure repeated volume changes. But when the stress exceeds the yield strength, the polymers' deformation belongs to plastic deformation, meaning that the strain cannot recover completely when the stress is removed and residual strain becomes permanent deformation. The ability of binders to limit volume change is thus diminished. Furthermore, when the stress exceeds the ultimate strength, polymers fracture and the binders fail.

In the face of the large volume change, the stress can be dissipated through the binder layer to alleviate the particle damage caused by particle expansion and extrusion. The molecular design offers effective strategies for binders that accommodate strong volume changes: (a) dissipate energy *via* sacrificial bonds and disperse accumulated stress *via* the branched configuration of the binders; (b) buffer the stress *via* the deformation and relaxation of highly elastic binders; and (c) overcome the repeated volume change *via* the dynamic bonds of intermolecular interactions to provide self-healing ability.

A method was proposed by Zhang *et al.* utilizing PAA and carboxylated nitrile butadiene rubber (XNBR) with tannic acid

(TA) as a cross-linker to construct a binder (named PTBR) for SiMP and  $\text{SiO}_x$  anodes.<sup>114</sup> This has gradient bonding energy as shown in Fig. 3c. Among these bonds, in addition to a series of reversible hydrogen bonds with different bonding energies as sacrificial bonds, covalent bonds are formed by the amidation reaction between the carboxyl groups of the binder and the amino groups of amino-functionalized carbon nanotubes to provide stronger bonding. With the volume variation of Si anodes, the hydrogen bonds dissociate successively to dissipate energy and disperse stress uniformly, which is profitable to reduce damage to the electrode from large volume expansion. The finite element modelling validated the conclusion that PTBR binders can indeed improve the uniform dispersion of stress in Si anodes during lithiation compared to PT binders (a mixture of PAA and TA) without XNBR (Fig. 3d). Atomic force microscopy (AFM) was used to characterize the stress dispersion by the plastic work of electrodes.<sup>75,114</sup> The average plastic work of SiMP/PTBR was smaller (0.991 keV) and dispersed even more than SiMP/PT (2.947 keV). Branched structures of dendrimers can disperse stresses because the tensile force,  $F$ , is dispersed through  $n$  branches, so the force on each branch is reduced to  $F/n$ .<sup>10</sup> Hyperbranched  $\beta$ -cyclodextrin polymers ( $\beta$ -CDp) can be used as binders.<sup>115,116</sup> Jeong *et al.* showed Si electrode surfaces with  $\beta$ -CDp had less cracks *via* scanning electron microscopy (SEM) compared with linear alginate binders.<sup>117</sup> In addition, Si anodes with  $\beta$ -CDp demonstrated better long cycling performance compared to linear binders, such as alginate and PVDF. The capacity retention of Si/ $\beta$ -CDp was 50.6% compared with Si/alginate (27.1%), whereas the capacity of Si/PVDF rapidly decayed during 25 cycles.

Owing to their high elasticity and flexibility, binder layers can buffer the strain/stress *via* deformation and relaxation. The Choi group designed a binder with a thread-ring structure in which polyrotaxane (PR)—comprising of polyethylene glycol (PEG) threads and  $\alpha$ -cyclodextrin ( $\alpha$ -CD) rings—is covalently integrated with PAA, and the binder is named PR-PAA.<sup>26</sup> According to physical principles, the movable PR is analogous to movable pulleys and can reduce the tensile force proportionate to the number of PR moieties, improving the ability to endure extreme stretching stress. Another feature was that the sliding motion of the molecular pulleys equalized the strain on the all-polymer chains in contrast to conventional cross-linking architecture, where the pressures were locally concentrated on shorter chains because the cross-linking sites were fixed. As shown in Fig. 3f, when the strain was small, the PAA chain rearranged along the load direction to buffer the stress. But with a further increase in strain, the ring sliding of PR played a dominant role to release the stress, which allowed PR-PAA films an astonishing maximum stretch up to 390%, while only 37% was found for PAA films. At a current density of 0.033 C, the initial discharge capacity of PR-PAA-based SiMP anodes was 2971 mA h  $\text{g}^{-1}$  with a coulombic efficiency of 91.22%, while the values are 2579 mA h  $\text{g}^{-1}$  and 81.61% for PAA-based anodes (Fig. 3j). At 0.2 C, PR-PAA-based SiMP





**Fig. 3** Modification strategies to accommodate volume changes of electrodes. (a) Typical problems induced by the electrode volume change. Reproduced with permission.<sup>9</sup> Copyright 2018, Royal Society of Chemistry. (b) Schematic representation of the stress-strain curves of polymers. (c) The gradient cross-linking bonds of PTBR binder. (d) The stress distribution of lithiated Si particles of  $\mu\text{Si}/\text{PT}$  and  $\mu\text{Si}/\text{PTBR}$  through the finite element simulation. (e) The distribution of plastic work on the surface of  $\mu\text{Si}/\text{PT}$  and  $\mu\text{Si}/\text{PTBR}$  from AFM. (c)–(e) are reproduced with permission.<sup>114</sup> Copyright 2019, Wiley. (f) Comparison of stress-strain curves of PR-PAA with PAA films, and schematic mechanical interaction of PR-PAA. (g) Initial charge/discharge profiles of the PR-PAA-SiMP and PAA-SiMP electrodes. (h) Discharge areal capacity of the PR-PAA-SiMP and PAA-SiMP electrodes over cycling. The inset is the coulombic efficiencies of PR-PAA-SiMP. (f)–(h) are reproduced with permission.<sup>26</sup> Copyright 2017, American Association for the Advancement of Science. (i) Chemical structure of the Spandex binder and illustration of hydrogen bonding between Spandex and Ag particles. (j) Schematic illustration of controlling the large volume change during lithiation and delithiation of the silver-carbon composite electrodes. (i) and (j) are reproduced with permission.<sup>43</sup> Copyright 2022, American Chemical Society. (k) Working mechanism of dynamic cross-linking of  $\beta\text{-CDp}$  and 6AD on a silicon surface. (l) Chemical structures of 6AD and 1AD. (m) Comparison of cycling performance based on different binders in Si electrodes. (k)–(m) are reproduced with permission.<sup>27</sup> Copyright 2015, American Chemical Society.



anodes maintained an areal capacity of  $2.43 \text{ mA h cm}^{-2}$  after 150 cycles, which is 91% of their initial capacity. In comparison, after 50 cycles, the PAA-based electrode only kept 48% of its initial capacity (Fig. 3h). The lithium metal anode, the ideal next-generation anode, is also faced with a large volume change during the deposition and dissolution of lithium. Carbon nanotubes (CNTs) can be employed as a 3D scaffold to guide uniform Li deposition and prevent Li-dendrite growth but easily suffer ruptures due to a large tensile stress generated during the lithium uptake–release cycles. Therefore, based on the same binder molecule, the Choi group used PR–PAA for lithium metal anodes to alleviate CNT fracturing and enhance the cycling stability.<sup>118</sup> The LFP–Li full cells with CNTs but without PR–PAA binders maintained 60% capacity retention after 50 cycles. In contrast, the cell with CNTs/PR–PAA maintained 65% capacity retention after 140 cycles. Another molecular design example is *via* the deformation of flexible polymer chains to release the stress. A binder comprised of soft and rigid chains, known as “Spandex”, was applied to a silver–carbon composite anode with large volume changes upon lithiation/delithiation.<sup>43</sup> The rigid chains consisting of ureido and phenyl structures were riveted on the surface of Ag *via* hydrogen bonding interactions. And the soft chains consisting of polyethylene glycol (O–R–O segment) endowed the binders with elastic adjustment (Fig. 3i). The soft segment can be stretched during lithiation, but is unstretched during delithiation, realizing the reversible change of the binder network structure (Fig. 3j). It has been demonstrated that the Spandex binders perform well in many electrode systems, including LFP<sup>119</sup> and NCM cathodes.<sup>120</sup>

Apart from anodes, cathode materials also undergo volume changes,<sup>42</sup> which become more severe in solid-state batteries due to the rigid solid–solid contact. Although a large pressure (over 50 MPa) is usually necessary in solid-state battery configurations to inhibit volume changes and retain the interfacial contact, it can be impractical for applications.<sup>121</sup> Gregory *et al.* synthesized a block polycarbonate binder to buffer the volume changes of NCM811 (~6%) in  $\text{Li}_6\text{PS}_5\text{Cl}$  electrolyte.<sup>65</sup> This binder demonstrated high tensile strain (1000% without breaking), excellent elastic recovery (~98.3%) and high compression resistance. Benefitting from the extraordinary elasticity, under a low pressure of 1 MPa, the solid-state batteries with the binder showed a capacity retention of over 90% after 80 cycles and over 70% after 500 cycles.

In addition to strong cross-linking (described in section 2.1), there is another type of cross-linking *via* weak intermolecular interactions, such as hydrogen bond interactions,<sup>81,88,122–124</sup> disulfide bond interactions,<sup>125</sup> host–guest coordinated interactions,<sup>27</sup> ionic interactions,<sup>38,126</sup> *etc.* The binding network constructed by strong cross-linking could be too rigid to sustain a large volume change. Comparatively, the weak cross-linking due to reversible and dynamic intermolecular connections endows the polymer with a self-healing ability. A polymeric binder comprising

hyperbranched  $\beta$ -CDp and a dendritic gallic acid cross-linker incorporating six adamantane units (6AD) was applied to silicon anodes.<sup>27</sup>  $\beta$ -CDp adhered on the surface of Si tightly *via* hydrogen bonds and was cross-linked by 6AD in which adamantane reversibly inserted into the cavities of  $\beta$ -CDp through host–guest interactions (Fig. 3k). In contrast, 1AD cannot cross-link with  $\beta$ -CDp. The molecular structures of 6AD and 1AD are shown in Fig. 3l. Adamantane was extracted from the cavities of  $\beta$ -CDp when the Si expanded but inserted into it when the Si contracted, which dynamically adjusted the network structures. In cycling tests, alginate, PAA and CMC showed rapid capacity decay, reaching only 21.7%, 25.2%, and 30.5% capacity retention, respectively, after 150 cycles, resulting from the linear structures and poor elastic properties. However,  $\beta$ -CDp/6AD retained capacity retention up to 90% after the same number of cycle. It is noteworthy that  $\beta$ -CDp/1AD only has a capacity retention of 23%, which proves that, despite host–guest interactions, the lack of a cross-linker cannot preserve the integrity of the electrodes (Fig. 3m). Polyurea consists of a urea ( $-\text{NH}-\text{C}=\text{O}-\text{NH}-$ ) structure, where dual hydrogen bonds ( $\text{N}-\text{H}\cdots\text{O}=\text{C}$ ) are formed. The abundant hydrogen bonds are sufficient and powerful enough to provide a self-healing ability and tension resistance. For example, Bao's group developed binders that included a urea structure (named as self-healing polymers (SHPs)) for Si anodes.<sup>81,123,124</sup> The strain of an SHP could reach 300% without breaking, and the self-healing phenomenon of electrodes with an SHP was observed. The initial discharge capacity and capacity retention of Si anodes with an SHP was  $2617 \text{ mA h g}^{-1}$  at  $0.4 \text{ A g}^{-1}$  and 80%, respectively, after 90 cycles.

Although a dynamic architecture through weak cross-linking is an efficient strategy to overcome volume changes, reversible bonds are in turn easy to break apart and hence cannot provide persistent mechanical strength during prolonged cycling. Lee *et al.* proposed an interesting concept of an “adaptive binder”.<sup>127</sup> Its backbone was polysaccharides (*e.g.*, hyaluronic acid (HA), CMC or alginate) grafted with gallol (GA) (1,2,3-trihydroxybenzene) moieties. When the volume of the SiMP changed in the early cycles, the binder would reposition and reorient *via* hydrogen bond cleavage and regeneration, leaving sufficient space to adapt to volume variation. Then, when the binder volume changes became relatively stable in the later cycles, the intermolecular interactions converted from reversible supramolecular interactions into irreversible covalent linkages. The fixed framework largely improved the structural stability of the electrode over prolonged cycling. Rheological tests showed the mechanical property of the slurry was obviously enhanced after 120 hours of aging because of the formation of covalent bonds. In order to compare the cyclability of HA–GA and HA as binders, SiMP anodes were tested in a half cell at 1 C. The HA–GA binder showed  $1153 \text{ mA h g}^{-1}$  capacity even at the end of the 600th cycle. But the HA binder exhibited a rapid decrease of capacity down to  $\approx 1000 \text{ mA h g}^{-1}$  at the 100th cycle and  $347 \text{ mA h g}^{-1}$  at the 600th cycle.





## 2.2 Mitigating interfacial degradation

Owing to the thermodynamic instability, a CEI or SEI will be formed on the contact between electrodes and electrolyte. A large number of reports have shown that the electrochemical performance of batteries is starkly related to the properties of the interphase layers. Therefore, how to construct efficient and stable CEIs and SEIs is a research focus.

In high-voltage transition-metal (TM) cathodes, there are particularly severe challenges to be faced with the interface. The continuous decomposition of the electrolyte at the cathode surface is considered to be one of the most important causes of interfacial degradation.<sup>128</sup> The electrolyte readily reacts with the cathode surface to produce the as-termed CEI.<sup>129,130</sup> In addition, various reactive intermediates from the electrolyte, such as HF, free radicals, *etc.*, can destroy the pristine CEI and trigger more side reactions. Additionally, the intrinsically unstable crystal structure at the cathode surface in the high delithiated state undergoes dissolution of TM ions and release of O<sub>2</sub>, inducing chemical crossover with the anode surface. In fact, in addition to the prevalent approaches of electrolyte design and electrode coating, the rational molecular design of binders has also proved to be an efficient strategy to mitigate the interfacial degradation.<sup>131</sup> Binders with a special design can uniformly coat the cathode surface with strong adhesion as an artificial CEI, and scavenge/absorb a variety of reactive intermediates to protect the surface structure and alleviate electrolyte decomposition to some extent. In addition, it is reported that the crystal structure of cathodes at the surface can be stabilized by the binders to inhibit TM-ion dissolution.

Li *et al.* used polyaniline (PANI) as a binder for ultrahigh-nickel layered oxide cathodes (LiNi<sub>0.94</sub>Co<sub>0.06</sub>O<sub>2</sub>) at 2.8–4.4 V.<sup>132</sup> Uniform and stable artificial CEIs were constructed at the surface of the cathodes. Time-of-flight secondary ion mass spectrometry (TOF-SIMS) results showed that the CEI of the PANI samples was regulated to a dual-layer structure consisting of inorganic (PO<sub>2</sub><sup>-</sup>/POF<sub>2</sub><sup>-</sup>) and organic (C<sub>2</sub>HO<sup>-</sup>) layers, which were thinner and more homogeneous compared to that of PVDF (Fig. 4a), and importantly, free of a transition-metal species layer (NiF<sub>3</sub><sup>-</sup>/CoF<sub>3</sub><sup>-</sup>). In contrast, the CEI of the PVDF samples featured a triple-layer structure, comprising inorganic species in the exterior layer, organic species in the intermediate layer and dissolved transition-metal species penetrating into the interior layer. A thin and stable artificial CEI ensures long-term cycling. The full cell of graphite/LiNi<sub>0.94</sub>Co<sub>0.06</sub>O<sub>2</sub> with PANI as a binder at C/2 rate and 25 °C exhibited 81% capacity retention after 1000 cycles, while that with PVDF only exhibited 47% capacity retention. The capture of various reactive intermediates, such as HF, free radicals and active oxygen, plays a critical role in stabilizing the cathode interphase. HF from the hydrolysis of LiPF<sub>6</sub> usually degrades the CEI. The imine nitrogen in PANI could be coordinated to F<sup>-</sup>,<sup>132</sup> and the sulfonic anion group in Nafion could attract H<sup>+</sup>,<sup>45</sup> both of which are helpful for scavenging HF from the decomposition of a lithium salt and solvents. A photostabilizer (PS) as an anti-aging binder additive

(shown in Fig. 4b) was proposed by Mu *et al.*, realizing the capture of free radicals from the electrolyte and active oxygen from the cathodes at high voltage.<sup>72</sup> The author designed delicate experiments to validate this anti-aging ability. When PS and PVDF were added to the free-radical detection reagent (1,1-diphenyl-2-picrylhydrazyl free radical) or to the <sup>1</sup>O<sub>2</sub> indicator (indocyanine green), the color of the solution became colorless from purple or green, but the sample but only PVDF did not, which proved the absorption of free radicals and active oxygen by the PS. Online differential electrochemical mass spectrometry (DEMS) results further indicated that the PS ameliorated the release of O<sub>2</sub> during operation (Fig. 4b). In addition, the agent has been demonstrated to have universal radical-capture abilities in various layered oxide-based cathodes, including NCM, LRMO, and LCO cathodes, and under different working conditions (Fig. 4c).

The irreversible migration of TM ions leads to a phase transition from layer phases to spinel phases or/and a rock-salt phase, accompanied by the dissolution of TM ions and release of O<sub>2</sub>. Jin *et al.* synthesized a DPGP-PEI/PVDF binder by cross-linking a functionalized terpolymer named as DPGP with polyethylenimine (PEI), and mixing with PVDF for use in NCM811 cathodes at 2.8–4.5 V.<sup>51</sup> The polar and electron-rich functional groups of DPGP-PEI, including catechol and amide groups, interact with the positive TM ions at the interfacial lattices, constraining the dissolution of TM ions to stabilize the surface structure. The high-angle annular dark-field scanning transmission electron microscopy (HAADF-STEM) results revealed that the surface of the PVDF-based NCM811 cathodes consisted of a rock-salt phase in the outer layer, a thick spinel phase in the intermediate layer and a layered phase in the bulk. In contrast, only a thin layer of spinel phase was formed on top of the layered structure of the DPGP-PEI/PVDF-based NCM811 cathode without the presence of the rock-salt phase (Fig. 4d). Furthermore, the XRD refinement results indicated a lower degree of Li/Ni cation mixing in the DPGP-PEI/PVDF-based NCM811 cathode. The working mechanism of DPGP-PEI/PVDF that mitigates the interfacial and structural degradation is illustrated in Fig. 4e. The TOF-SIMS showed that the cycled graphite anode surface with DPGP-PEI/PVDF exhibited lower content of Co, Mn and Ni ions than that with PVDF, demonstrating that DPGP-PEI suppresses ion dissolution and cathode-to-anode crossover. LRMO cathodes with high capacities over 200 mA h g<sup>-1</sup> are more prone to surface degradation of the lattice structure because of the involved oxygen redox reaction, where the vacancies left from the released O are easily captured by TM ions, accelerating the irreversible migration of TM ions. According to the work of Xu *et al.*, polyacrylonitrile (PAN) was used as the binder for LRMO cathodes, which coordinates with positive TM ions at the surface through CN triple bonds to prevent TM ion migration.<sup>23</sup> Density functional theory calculations showed the energy barrier of Mn ion migration in delithiated LRMO cathodes was lower (+2.58 eV) with PAN than that without PAN (+3.59 eV) (Fig. 4f). Remarkably, the energy barrier of Ni





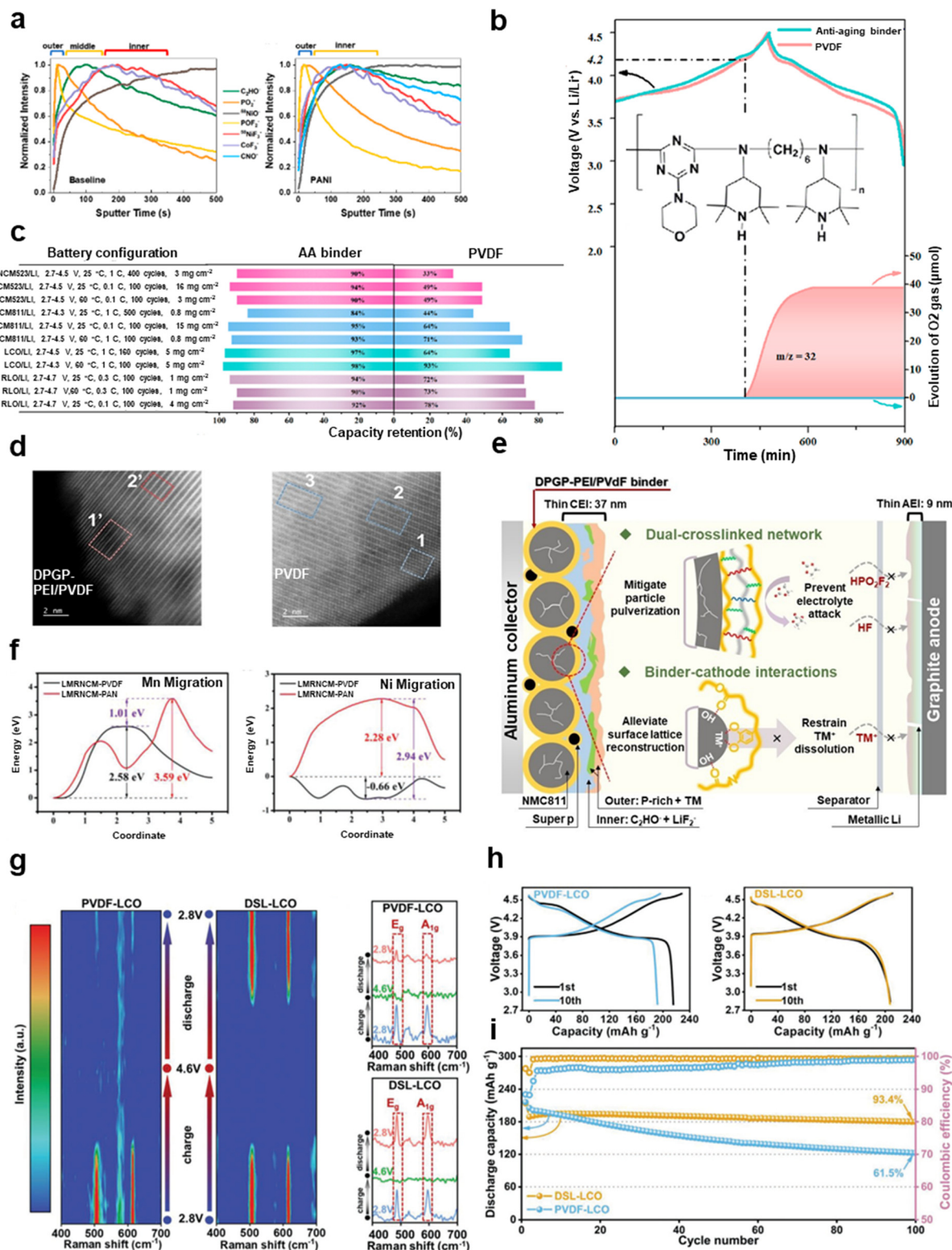


**Fig. 4** Modification strategies to mitigate interphase degradation. (a) Interfacial components of cathodes with PVDF and PANI. Reproduced with permission.<sup>132</sup> Copyright 2020, American Chemical Society. (b) O<sub>2</sub> evolution of NCM811/Li half cells with PVDF and anti-aging binders in the online DEMS system. (c) Capacity retention of various electrode systems under various test conditions with PVDF and the anti-aging binder. (b) and (c) are reproduced with permission.<sup>72</sup> Copyright 2021, American Chemical Society. (d) HAADF-STEM images of the DPGP-PEI/PVDF- and PVDF-based NCM811 particles after 1000 cycles. (e) TM-ion scavenging mechanism of DPGP-PEI/PVDF and the chemical structure of DPGP (inset). (d) and (e) are reproduced with permission.<sup>51</sup> Copyright 2023, Wiley. (f) The migration energy barriers of Mn and Ni with or without PANI binder. Reproduced with permission.<sup>23</sup> Copyright 2022, Wiley. (g) *In situ* Raman evolution of PVDF-LCO and DSL-LCO at the E<sub>g</sub> and A<sub>1g</sub> peaks during the first cycle. (h) The charge-discharge curves of PVDF/LCO and DSL/LCO at the first and 10th cycles. (i) The cycling performance of PVDF/LCO and DSL/LCO during 100 cycles at 0.5 C. (g)–(i) are reproduced with permission.<sup>22</sup> Copyright 2021, Wiley.



ion migration in delithiated LRMO cathodes without PAN is  $-0.66$  eV, which meant favorable Ni ion migration. However, the migration barrier of Ni ions rose to  $+2.28$  eV with PAN, meaning ion migration was inhibited effectively (Fig. 4f). Huang *et al.* designed dextran sulfate lithium (DSL) binders to enhance the interaction with the LCO surface by sulfonic anion groups, which could suppress the detrimental phase transition from the O3 phase to the H1-3 phase.<sup>22</sup> *In situ* Raman spectroscopy showed that the PVDF/LCO electrode exhibited obvious attenuation in the  $E_g$  (O-Co-O bending vibration) and  $A_{1g}$  (Co-O stretching vibration) peaks, while the DSL/LCO cathode showed reversible evolution of the  $E_g$  and  $A_{1g}$  peaks during the first cycle from 2.8 V to 4.6 V (Fig. 4g). This was attributed to the interaction between DSL and LCO that greatly prevents the irreversible breaking of Co-O and O-Co-O bonds at the surface, and further suppresses the deep-going structural collapse during the high-voltage LCO cycling. Fig. 4h shows the discharge curves of the first and tenth cycles for high-voltage LCO and Fig. 4i shows the cycling performance of PVDF/LCO and DSL/LCO at 0.5 C. DSL/LCO retained a higher capacity retention of 93.4% after 100 cycles compared to PVDF/LCO (61.5%).

There are also many challenges at the anode interphase, such as large impedance, structural instability, *etc.* Likewise, an effective SEI can be constructed using a binder coating to alleviate the decomposition of electrolyte at the interface.<sup>133-135</sup> A functional binder can modify the SEI composition *via* an electrochemical reaction to improve the electrical and mechanical properties of the SEI, facilitating the electrochemical performance of batteries.<sup>68</sup> Pradhan *et al.* synthesized a B-bearing caffeic acid-based binder for graphite anodes.<sup>136</sup> Compared with the solvent and salts, the lower unoccupied molecular orbital (LUMO) energy level of this binder could facilitate the preferential reduction to form a borate-rich SEI. The borate-rich SEI decreased SEI resistance and improved the electrode dynamics. Furthermore, it is reported by Wang *et al.* that due to a lower LUMO energy level, a poly(vinylamine) (PVAm) binder containing amino ( $-NH_2$ ) and amide ( $-NH-CHO$ ) groups could also be preferentially reduced and form an N-rich SEI that is Li-conductive and has good mechanical properties.<sup>137</sup> The Li 1s X-ray photoelectron spectroscopy (XPS) spectra verified the presence of Li-N at the Si/PVAm surface. Consequently, it was further proved by the electrochemical impedance spectroscopy (EIS) that Si/PVAm ( $52 \Omega$ ) exhibited lower interfacial impedance in comparison to Si/PVA ( $65 \Omega$ ) and Si/PVDF ( $123 \Omega$ ), which is attributed to the N-rich SEI. A cycling test of the Si anodes was performed to investigate the influence of PVAm. Si/PVAm delivered  $2000 \text{ mA h g}^{-1}$  capacity after 200 cycles, while Si/PVDF and Si/PAA only delivered 66 and  $820 \text{ mA h g}^{-1}$  capacity, respectively, after the same number of cycles.

## 2.3 Electrical properties

**2.3.1 Improvement of electrical conductivity.** Low electrical conductivity is the bottleneck of rate performance

of the active materials.<sup>138,139</sup> Although added conductive carbons can enhance the electrical conductivity of electrodes, large volume changes during cycling lead to the loss of contact between the conductive carbons and the active materials (Fig. 5a).<sup>9</sup> If binders are endowed with the ability to conduct electrons then, benefitting from the flexibility of the binders, the electrical pathway can always be guaranteed despite drastic volume changes. The conductive binder represents a pivotal application scenario to possibly avoid the use of conductive carbon (Fig. 5a).<sup>140</sup> Generally, electrically conductive polymers have a conjugate structure with alternating single and double bonds, and a lower energy gap between the bonding orbitals and antibonding orbitals than that of a non-conjugate structure and thus delocalized  $\pi$  electrons can be transported directionally under an electric field. The introduction of polarons through redox or doping can further reduce the energy gap and realize the satisfactory conductivity of the conducting polymers (Fig. 5b). In contrast, it is well known that PVDF is electrically insulating due to its non-conjugated structure.

Conductive polymers are typified by polyfluorene, polythiophene, polyaniline, polypyrrole, and so on. The most obvious way to design conductive binders is to imitate these conductive polymers as molecular backbones that are supposed to ensure the adhesion property. Liu's group chose poly(9,9-dioctylfluorene-*co*-(9H-fluorene)) (HPF) as the baseline and introduced carbonyl groups into the fluorene units, producing poly(9,9-dioctylfluorene-*co*-fluorenone) (PF), to regulate HPF's LUMO energy level. The decreased energy level difference enhances the electrical conductivity. Based on this method, they developed a series of n-type polyfluorene-based multifunctional binders, such as poly(9,9-dioctylfluorene-*co*-fluorenone-*co*-methylbenzoic ester) (PFM) and poly(9,9-di(oxy-2,5,8-trioxadecane) fluorene-*co*-(9,9-dioctylfluorene)-*co*-methylbenzoic ester) (PEFM) (Fig. 5c).<sup>32,141-143</sup> The high conductivity ( $\sim 1 \times 10^{-6} \text{ S cm}^{-1}$ ) of these binders contributes to the superior electrochemical performance. More importantly, an inspiring strategy that manipulates the properties of polymers by producing hierarchically-ordered structures (HOS) was proposed.<sup>32</sup> As we know, proteins achieve advanced functionality by forming higher-order structures, through processes such as structural folding and multi-molecule arrangement, whereas advanced functionality is impossible with primary structures alone. Similarly, the removal of alkyl or alkoxy side chains of polyfluorene-based binders by thermal treatment could enhance the  $\pi$ - $\pi$  interactions between chain segments and hence build HOS of the binders. A schematic diagram of HOS is shown in Fig. 5d. This strategy extended the ordered range of the microstructure and reduced the amorphous intercrystallite regions, where carriers are expected to move more efficiently. Abundant micro-crystal orientations in HOS-PFM due to  $\pi$ - $\pi$  stacking between the aromatic chains were observed directly by four-dimensional scanning transmission electron microscopy (4D-STEM) (Fig. 5e). As a result, this seemingly simple method significantly improved the mechanical properties, electric ( $\sim 0.1 \text{ S cm}^{-1}$ ) and ionic (a



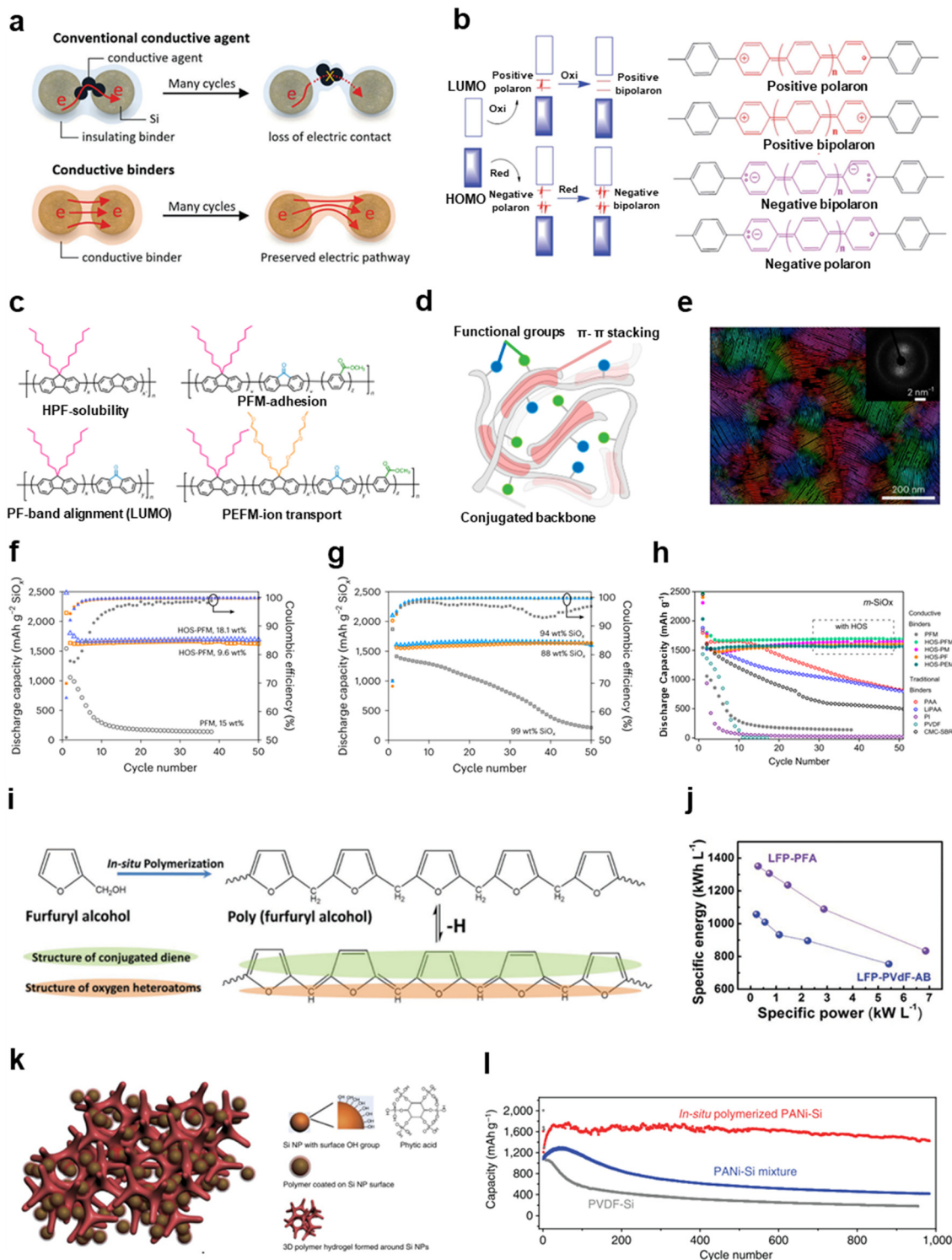


**Fig. 5** Modification strategies to improve the electronic conductivity of electrodes through functional binders. (a) Comparison of conventional conductive agents and conductive binders during volume changes. Reproduced with permission.<sup>9</sup> Copyright 2018, Royal Society of Chemistry. (b) The electrically conductive mechanism of a conjugated polymer through polaron transport. Reproduced with permission.<sup>154</sup> Copyright 2015, Royal Society of Chemistry. (c) Structural formula of the polyfluorene-based multifunctional conductive binders. (d) Schematic diagram of HOS binders with higher-order structures. (e) Micro-crystal orientations of HOS-PFM from 4D-STEM. (f) Battery cycling of m-SiO<sub>x</sub> anodes with PFM and HOS-PFM (9.6 wt% and 18.1 wt%). (g) Cycling performance of high-content m-SiO<sub>x</sub> anodes (88 wt%, 94 wt% and 99 wt%) without conductive carbon additives but with HOS-PFM. (h) The comparison of cycling performances of m-SiO<sub>x</sub> anodes with various binders during 50 cycles. (c)–(h) are reproduced with permission.<sup>32</sup> Copyright 2023, Springer Nature. (i) Chemical structure of conjugated PFA. (j) The relationship of power density and volumetric density with PFA- and PVDF-based LFP electrodes. (i) and (j) are reproduced with permission.<sup>149</sup> Copyright 2019, Wiley. (k) Graphical illustration of an *in situ* polymerized conductive adhesive network. (l) Cycling performance of *in situ* polymerized PANI/Si and PVDF/Si. (k) and (l) are reproduced with permission.<sup>150</sup> Copyright 2013, Springer Nature.





$\text{Li}^+$  diffusion coefficient of  $1.2 \times 10^{-11} \text{ cm s}^{-1}$ ) conductivity of the binders by constructing higher-order structures without introducing new functional groups. The cycling performance of the HOS-PFM-based microparticle  $\text{SiO}_x$  (m- $\text{SiO}_x$ ) anodes was significantly better than PFM despite the lower content of HOS-PFM (9.6 wt%) (Fig. 5f). The high-loading HOS-PFM-based m- $\text{SiO}_x$  (88 wt%, 94 wt% and 99 wt%) still retained high coulombic efficiency and capacity retention without any conductive carbons (Fig. 5g). Fig. 5h shows that the electrochemical performance of polyfluorene-based conductive binders (HOS-PFM, HOS-PM, HOS-PF and HOS-PEM) can be significantly improved by the HOS strategy in stark contrast to the conventional binders (PAA, LiPAA, PI, PVDF and CMC/SBR) and non-HOS binders (PFM).

Polythiophene, a common conductive polymer, can also be used as the backbone of multifunctional binders. Introducing long alkane chains<sup>144–146</sup> or Li-ionized alkyl carboxylate groups with various lengths<sup>20,147</sup> into polythiophene, can increase both ionic and electronic conductivities. These binders exhibit exceptional electrochemical performances in a wide variety of electrode systems, such as graphite,<sup>147</sup> silicon<sup>147</sup> and  $\text{Fe}_3\text{O}_4$  (ref. 20) anodes, as well as  $\text{V}_2\text{O}_5$  (ref. 144 and 146) and LFP<sup>145</sup> cathodes. Another well-explored thiophene-based polymer, namely poly(3,4-ethylene dioxythiophene) doped with poly(styrene sulfonate) (PEDOT:PSS), was also exploited as a binder. Higgins *et al.* investigated the effect of formic acid (FA) doping on the conductivity of PEDOT:PSS and optimized the content of FA (10%).<sup>148</sup> The cycling tests showed PEDOT:PSS/SiNP with 10% FA has the highest specific capacity of  $2681 \text{ mA h g}^{-1}$  in the second cycle and  $1950 \text{ mA h g}^{-1}$  at the 100th cycle in comparison to CB/LiPAA, PEDOT (no FA) and PEDOT (5% FA). Because of the enhancement of electrical conductivity, PEDOT:PSS/SiNP exhibited superior rate performance compared to other binders.

*In situ* polymerized PFA as a conductive binder has been employed in LFP electrodes.<sup>149</sup> The extended conjugated regions were beneficial to decreasing the energy gap between the HOMO and LUMO and hence improve the conductivity (Fig. 5i). From Fig. 5j, it is evident that the PFA binder affords the LFP electrode a higher energy density and power density compared to PVDF. Furthermore, the *in situ* polymerized PANI cross-linked with phytic acid constructed a 3D conductive network for Si anodes (Fig. 5k).<sup>150</sup> The *in situ* PANI/SiNP composite electrodes exhibited a relatively stable reversible capacity of  $1600 \text{ mA h g}^{-1}$  after 1000 cycles. In comparison, PVDF/SiNP and the mixed PANI/SiNP have rapid capacity decay (Fig. 5l). Moreover, polypyrrole (PPy) can also be employed as a conducting binder. The *in situ* polymerized and cross-linked PPy formed a conductive gel framework, which demonstrated superior electrochemical performance in Si and  $\text{Fe}_3\text{O}_4$  anodes.<sup>151,152</sup>

In addition to the use of conducting polymers as the backbone of binders, the electronic conductivity can also be improved by grafting large conjugated fragments. For example, molecules of the polycyclic aromatic hydrocarbon

pyrene were grafted onto polyacrylate as side chains.<sup>153</sup> The pyrene groups are close enough together to readily self-assemble into an ordered structure, which can further improve the electrical conductivity due to stacking of the aromatic moieties. Furthermore, an inorganic composite binder made of carbon nanotubes interwoven in cellulose was proposed.<sup>84</sup> Benefitting from ultra-high electrical conduction ( $816 \text{ S m}^{-1}$ ) of the inorganics, electrodes with this binder possessed superior rate capability. At high current density ( $10 \text{ mA cm}^{-2}$ ), LCO with this binder delivered  $2.6 \text{ mA h cm}^{-2}$  capacity, but LCO with PVDF barely has capacity due to the polarization.

**2.3.2 Improvement of ionic conductivity.** Analogous to the electronic conductivity, ionic conductivity plays a fundamentally important role in the kinetics of electrode processes and rate capability.<sup>155,156</sup> Improving the ionic conductivity of liquid- or solid-state electrolytes, and active materials is the prevalent approach to this issue. Ionically conductive binders, due to their flexibility and elasticity, can easily adapt to deformation and sustain the continuous ionic pathway, especially in all solid-state batteries. Therefore, the ionically conductive binders can provide sustained ionic conduction in spite of large volume changes, while other components in the electrode cannot. In a similar manner to the polymer electrolyte, electron-rich polar moieties on the binders can coordinate with dissociated  $\text{Li}^+$ . In the amorphous region of polymers, orientational interchain or intrachain transport of  $\text{Li}^+$  under an electron field is therefore realized by the wiggling of the chain (Fig. 6a).<sup>157</sup> Moreover, polyelectrolyte<sup>126,158</sup> or polyanion<sup>159</sup> binders can also enhance lithium-ion conduction because the anions are fixed on the polymer and hence cations (*e.g.*,  $\text{Li}^+$ ) are only involved in oriental migration (Fig. 6a). Actually, PVDF can absorb certain amounts of electrolyte and acquire ionic conductivity. However, the ionic conductivity is relatively low, and the swelling in turn impairs the adhesion of PVDF.

Reducing the crystallinity and increasing the amorphous region is one of the efficient ways to increase the ionic conductivity of polymers. Increasing the degree of bifurcation of the polymer weakens the interactions between the chain segments and prevents the orientational alignment of the linear chains, which can reduce the crystallinity of the polymer. Jiang *et al.* grafted alkoxy chains onto linear PAA to reduce the crystallinity of PAA.<sup>160</sup> The degree of polymerization, molecular weight and  $T_g$  of the binders were regulated by the proportion of PAA and the cross-linker, tetra(ethylene glycol) diacrylate (TEGDA). The higher the cross-linker content, the lower the degree of polymerization and  $T_g$ , which evidenced more amorphous regions and higher ionic conductivity. The feed ratio of TEGDA and acrylic acid increased from 0 to 0.2, and  $T_g$  decreased from  $109.0$  to  $87.2$  °C. The ionic conductivity of a series of binders increased from  $5.77 \times 10^{-5}$  to  $5.01 \times 10^{-4} \text{ S cm}^{-1}$ . As the degree of branching in the binders increased, the interfacial resistance decreased and the capacity retention of the corresponding Si anodes increased.







**Fig. 6** Modification strategies to improve the ionic conductivity of electrodes through functional binders. (a) Schematics showing the ionic conduction mechanism of polymers. Reproduced with permission.<sup>157</sup> Copyright 2021, Royal Society of Chemistry. (b) The internal resistance of PVDF- and BBP-based NCM811 cathodes at different SOCs, and the structural formula of the BBP (inset). (c) Swelling tests of PVDF and BBP films. (d) Rate performance of PVDF- and BBP-based NCM811 cathodes. (b)–(d) are reproduced with permission.<sup>19</sup> Copyright 2022, Wiley. (e) Cycling performance and (f) initial coulombic efficiency of Si anodes with different binders. (g) Areal capacity and coulombic efficiency of high-mass-loading Si anodes with N-P-LIPN binders ( $28.88 \text{ mg cm}^{-2}$ ) during cycling. (e)–(g) are reproduced with permission.<sup>28</sup> Copyright 2020, Wiley. (h) Schematic diagram of electrolyte-free electrodes with ionically conductive binders. (i) The comparison of rate performance of electrolyte-free electrodes with Li-CMC and Na-CMC as binders. (j) Comparison of volumetric capacities of the electrolyte-free electrodes with Li-CMC and Na-CMC and composite electrodes. DFT calculation of Li diffusion energy with Na-CMC and Li-CMC in the (k) in-plane and (l) out-of-plane directions. (h)–(l) are reproduced with permission.<sup>162</sup> Copyright 2022, Elsevier.



The grafting of flexible and ionically conductive chains, such as alkoxy chains and amino groups, onto binders can also enhance ionic conductivity. For instance, a multifunctional amphiphilic bottlebrush polymer (BBP) was synthesized by Kim *et al.*, which consisted of polynorbornene and PAA.<sup>19</sup> The structural formula is shown in Fig. 6b. Due to the introduction of the acrylic moieties, the ionic transport and adhesive strength were simultaneously enhanced by the electron-rich carboxyl group. The galvanostatic intermittent titration technique (GITT) results showed that the internal resistance of BBP/NCM811 is lower than PVDF/NCM811 at different state of charge (SOC) values (Fig. 6b). At the same time, unlike PVDF, which realizes ionic conductivity through electrolyte uptake, BBP circumvents the damage of swelling to the structural stability and weakened adhesion of the binders due to the rigid structure of cyclopentane. Swelling tests showed the volume change of the BBP film is smaller than for PVDF (Fig. 6c). As a consequence, BBP/NCM811 demonstrated improved rate capability from 0.2 C to 3 C higher than PVDF/NCM811 (Fig. 6d). Another example is dopamine-grafted PAA mixed with PVA as a multifunctional binder (PAA-DA/PVA) for Si anodes.<sup>161</sup> Both GITT and EIS tests indicated that Si@PAA-DA/PVA had superior dynamical properties to Si@PAA/PVA and Si@CMC/SBR, as successive amide groups on the side chains could accelerate the transport of lithium ions.

Introducing ionized functional species, especially Li<sup>+</sup>, into the binders, namely polyanion binders, has also been shown to facilitate the transport of Li<sup>+</sup>. Li *et al.* mixed partially lithiated PAA and partially lithiated Nafion (NF) as a binder (N-P-LiPN) for Si anodes.<sup>28</sup> The lithium-ionized functional groups reduced the ionic diffusion barrier and increased ionic conductivity.<sup>162,163</sup> At 0.2 C, N-P-LiPN/Si exhibited a discharge capacity of 2143 mA h g<sup>-1</sup> after 100 cycles (Fig. 6e). Fig. 6e showed that the non-lithiated binders (N-PN, PAA and NF) possessed inferior capacity retention compared to the lithiated binders (N-P-LiPN, P-LiPAA and P-LiNF). And the individual binders (P-LiPAA, P-LiNF, PAA and NF) are all inferior to the mixed binders (N-P-LiPN and N-PN), which indicates the synergistic function of the lithiated binders. Most notably, N-P-LiPN/Si exhibits the highest initial coulombic efficiency of 93.18% (Fig. 6f). Furthermore, ultra-high-mass-loading Si anodes (28.8 mg cm<sup>-2</sup>) delivered an areal capacity of 49.59 mA h cm<sup>-2</sup> with cyclability of 30 times (Fig. 6g). Sulfonated poly(styrene) (SPS) ionomers were grafted onto poly(vinylidene fluoride-*co*-trifluoroethylene) (PVDF-TrFE) for MoS<sub>2</sub> electrodes.<sup>95</sup> The SPS formed ionic channels by self-assembly to facilitate ionic transport. At a current density of 0.5 A g<sup>-1</sup>, MoS<sub>2</sub> with PVDF-TrFE-*g*-SPS binders delivered a discharge capacity of 862.0 mA h g<sup>-1</sup> and retained 91.0% capacity after 1000 cycles compared with a 450.1 mA h g<sup>-1</sup> discharge capacity and ≈69% capacity retention of PVDF-TrFE binders.

Specially, Shin *et al.* synthesized a Li-CMC binder by substituting Na<sup>+</sup> in Na-CMC with Li<sup>+</sup> to improve the ionic conductivity.<sup>162</sup> There was no obvious difference between Na-

CMC and Li-CMC in a conventional liquid electrolyte for graphite electrodes because the ionic transport between electrodes was mostly realized by the electrolyte. But when applied in all-solid-state batteries without a solid electrolyte, the ionic transport was entirely dependent on the conductive binder inside the electrodes (Fig. 6h). The Li-CMC/SBR/graphite electrode delivered a higher capacity than the Na-CMC/SBR/graphite electrode (Fig. 6i). These electrolyte-free electrodes can achieve higher volumetric capacities compared with the composite electrodes with a solid electrolyte, because composite electrodes are thicker in the presence of additional, substantial electrolyte inside the electrodes (Fig. 6j). Molecular dynamics simulations indicated the faster lithium-ion diffusion kinetics in Li-CMC than in Na-CMC, especially along the out-of-plane direction (Fig. 6k and l).

## 2.4 Thermal properties

**2.4.1 Improvement of thermal safety and wide-temperature operability.** Battery thermal safety is affected by many factors, such as the electrolyte, while less attention is paid to the binders. How binders affect thermal safety and how to improve thermal safety through binder design, including preventing thermal runaway and battery combustion under abusive conditions such as overcharging, are worth consideration.<sup>164</sup> In addition, there are specific application scenarios that require the battery to operate in a wide range of temperatures, which puts additional requirements on the binders. These above-mentioned issues are associated with the binder's intrinsic thermal property.<sup>165</sup> As shown in Fig. 7a, with increasing temperature, the thermal disturbance of the polymeric chain is enhanced, which changes the mechanical properties of the polymers. When the temperature exceeds the viscous flow temperature ( $T_f$ ), polymers change from a high elastic state to a viscous flow state, and the wettability increases but the mechanical strength decreases. The  $T_f$  data of some common binders have been collected, including for PVDF (160 °C),<sup>77</sup> PTFE (327 °C),<sup>78</sup> PEO (65 °C).<sup>166</sup> As a result of the change in state, the fluidity of the polymers increases, and it is hard for the binders to maintain their structural integrity. More importantly, once exceeding the decomposition temperature ( $T_d$ ), the polymer begins to decompose, and the binders completely fail to work, affecting the battery safety. On the other hand, at low temperature, when the temperature is lower than  $T_g$ , the polymer chains gradually freeze and the polymer begins to crystallize, resulting in a loss of viscoelasticity and interface affinity, which means the polymer is no longer capable of binding the electrodes together.

How binders affect the thermal safety of batteries has been studied in detail by Gribble *et al.*<sup>55,167</sup> The influence of PVDF binders integrated with carbon black (CB) on the thermal stability of graphite anodes was investigated in comparison to PEDOT:PSS.<sup>55</sup> The differential scanning calorimetry (DSC) results for lithiated and electrolyte-wetted graphite anodes with PVDF/CB, PEDOT:PSS or PEDOT:PSS/CB showed that the heat from SEI decomposition was 143 J g<sup>-1</sup>,





**Fig. 7** Modification strategies to improve thermal stability of electrodes through functional binders. (a) Schematic diagram of the deformation-temperature curve of polymers. (b) Decomposition temperatures of PVDF and PI-FTD. (c) DSC curves of charged NCM811 with PVDF and PI-FTD binders. (b) and (c) are reproduced with permission.<sup>168</sup> Copyright 2019, Elsevier. Voltage and temperature profiles of 1 A h pouches comprising (d) PVDF@NCM and (e) PI@NCM overcharged to 10 V. The insets are the digital photographs of the pouch cells after overcharge. (d) and (e) are reproduced with permission.<sup>169</sup> Copyright 2016, Elsevier. (f) Schematic showing the flame-retardant mechanism of APP-based sulfur electrodes. Surface morphology of (g) S-APP and (h) S-PVDF electrodes after burning. (f)–(h) are reproduced with permission.<sup>92</sup> Copyright 2018, American Chemical Society. (i) Graphical illustration of the inorganic adhesive framework of UCFR and its special functions. (j) The dimensional evolution of Al, PVDF/LFP and UCFR/LFP at different temperatures. (k) Photographs of PVDF/LFP and UCFR/LFP on a flame. (l) Cyclability of UCFR/LFP after thermal treatment at 750 °C. (m) Cyclability of UCFR/LFP at different temperatures ranging from RT to 160 °C. (i)–(m) are reproduced with permission.<sup>85</sup> Copyright 2019, Wiley.





37.5 J g<sup>-1</sup> and 102 J g<sup>-1</sup>, and the total heat was 2.13 kJ g<sup>-1</sup>, 1.51 kJ g<sup>-1</sup>, 1.93 kJ g<sup>-1</sup>, respectively. The reason for this difference was that PEDOT:PSS with a lower specific surface area than carbon black has less electrolyte absorption and heat release. Moreover, a more stable and thinner SEI was formed on the surface of the electrodes with PEDOT:PSS, which raises the initial decomposition temperature and reduces the heat release from SEI decomposition. A similar thermal issue was reported by Pham *et al.* through binder design.<sup>168</sup> As a special engineering plastic, polyimide exhibits many special properties, such as high mechanical strength and thermal stability, which can be used in the design of thermally stable binders. A fluorinated polyimide (PI-FTD) binder containing trifluoromethyl and phthalimide structures was synthesized,<sup>168</sup> and thermogravimetric analysis indicated the decomposition temperature of PI-FTD was up to 500 °C, while that of PVDF was 433.8 °C (Fig. 7b). The DSC test of NCM811 cathodes charged to 4.4 V showed that the exothermal heat of PVDF/NCM811 was higher and the initial exothermal temperature of PVDF/NCM811 was lower than PI-FTD/NCM811 (Fig. 7c). In addition to the improved thermal stability of the binder itself, the protection of the electrode surface by PI-FTD and the construction with a stable CEI was also responsible for the improved thermal safety of the electrodes. Overcharging, as a kind of electrical abuse, is a concern with regard to the thermal safety of practical battery operation, and can lead to a risk of thermal runaway. Qian *et al.* utilized a polyimide binder, which also contained a key phthalimide structure, to restrain the thermal runaway of pouch cells with NCM cathodes.<sup>169</sup> When the batteries were charged to 10 V, the temperature of polyimide binder/NCM was just 80 °C, while that of PVDF/NCM reached 1000 °C (Fig. 7d and e).

Some specific binders with flame-retardant characteristics can significantly enhance battery safety. It was proposed by Zhou *et al.* that ammonium polyphosphate (APP) could be employed as a flame-retardant binder for sulfur cathodes.<sup>92</sup> The flame-retardant mechanism arose due to the presence of decomposition products of APP, including water and nonflammable NH<sub>3</sub>, that lowered the reaction temperature and cut off the supply of oxygen. Meanwhile, an insulating polymer layer was formed on the electrode surface that further retarded the spread of the flames (Fig. 7f). The XPS results indicated that the S-signal intensity on the surface of S/APP remained unchanged after burning. But a greater C signal and lower S signal was detected on the S/PVDF surface, which possibly resulted from the carbonization of organic matter and the volatilization of S. SEM results showed that porous structures were found on the surface of S/PVDF after combustion, while the surface of S/APP was uniformly coated (Fig. 7g and h). Some biopolymers have also been proved to have a flame retardant ability. Tragacanth gum (TG) as the binder of sulfur cathodes prevented the burning of a S/TG electrode even at temperatures over 180 °C.<sup>74</sup> The authors argued that, in the presence of abundant hydroxy groups, as the temperature increased the biopolymers underwent

dehydration–condensation reactions. The as-formed inert coating effectively blocks the positive electrode from the flame. Furthermore, phosphides and nitrides (*e.g.*, polyphosphonitrile) are considered to have good thermal stability and are commonly used as flame-retardant materials. A eugenol phosphazene (EP) binder was synthesized by Monisha *et al.* for sulfur cathodes.<sup>170</sup> With the increase of EP content, the specific ignition time, specific self-extinguishing time and limiting oxygen index of EP/S all decreased, demonstrating that EP efficiently reduced the flammability of S cathodes. The XPS results showed that the N=P signal disappeared after combustion, but the S signal was preserved. It is proposed that phosphazene was decomposed into polyphosphoric acids, carbonaceous char and gases (*e.g.*, N<sub>2</sub> and NH<sub>3</sub>), which inhibited further combustion. Likewise, a flame-retardant framework was constructed with cross-linked hexachlorocyclotriphosphazene in the binder.<sup>171</sup> The S/C cathodes with this binder could withstand a high temperature of 250 °C and not be ignited.

In contrast to most binders made of organics, inorganic binders have higher thermal stability and nonflammability while ensuring adhesion. Interestingly, an ultrahigh-capacity and fire-resistant (UCFR) inorganic adhesive framework comprising hydroxyapatite nanowires (HAP), conductive carbons and carbon fibers, was proposed by Li *et al.*<sup>85</sup> Unlike polymers where intermolecular interactions occur between functional groups, the inorganic framework maintained structural integrity through electrostatic self-assembly, as shown in Fig. 7i. Benefitting from the powerful electrostatic attraction, the UCFR/LFP cathodes had an extremely high loading (108 mg cm<sup>-2</sup>) and areal capacity (16.4 mA h cm<sup>-2</sup>). Moreover, owing to the high content of conductive material in the binder, this inorganic framework had ultra-high conductivity (3.69 S cm<sup>-1</sup>), so it can be directly used as flexible electrodes without a current collector. More importantly, this inorganic framework can endure extremely high temperatures. As shown in Fig. 7j, large areas of Al foil and PVDF/LFP had decomposed at 1000 °C, but UCFR/LFP basically had almost no change. A more direct experiment showed that UCFR/LFP electrodes maintained dimensional and current continuity on the flame over 10 min, while PVDF/LFP is burnt out after 10 s (Fig. 7k). Even after heat treatment at 750 °C, UCFR/LFP still maintained electrochemical activity and could be charged and discharged reversibly (Fig. 7l), which was almost impossible for conventional organic binder-based electrodes. Even at the high temperature (160 °C), UCFR/LFP could satisfy high-rate (2 C) working (Fig. 7m).

As the temperature decreases, the properties of binders change significantly. For example, thermal motion of chains is suppressed and polymers transfer from the high-elastic state to the glass state below  $T_g$ , which heavily impair the adhesive ability of the binders. Eom *et al.* compared PVDF and CMC/SBR as the cathode binders for a 2 A h NCM523/graphite pouch battery at low temperature.<sup>93</sup> In fact, the  $T_g$  of PVDF (-35 °C) was lower than for CMC/SBR (-5 °C), which





means PVDF does not crystallize at lower temperature ( $-35\text{ }^{\circ}\text{C}$ ) and maintains its viscoelastic property. Furthermore, from  $-30\text{ }^{\circ}\text{C}$  to  $45\text{ }^{\circ}\text{C}$ , PVDF had higher electronic conductivity than CMC/SBR. At  $-30\text{ }^{\circ}\text{C}$ , the anodes with PVDF discharged more capacity ( $0.86\text{ A h}$ ) than CMC/SBR ( $0.79\text{ A h}$ ). The cycling performance at low temperature ( $-10\text{ }^{\circ}\text{C}$ ) showed the PVDF-based battery maintained  $0.6\text{ A h}$  capacity after 100 cycles, while the CMC/SBR-based battery only had  $0.4\text{ A h}$ . It has also been shown that polyaniline was used as a binder for  $\text{LiNi}_{0.94}\text{Co}_{0.06}\text{O}_2$  cathodes, which can discharge at low temperature ( $-20\text{ }^{\circ}\text{C}$ ) and high rate ( $5\text{ C}$ ), contributing to the high conductivity of polyaniline.<sup>132</sup>

## 2.5 Dispersion properties

**2.5.1 Improvement of electrode homogeneity.** Electrodes generally consist of active materials, conductive carbons, binders, and voids filled with liquid or solid electrolytes. Whether these components are uniformly dispersed has a huge impact on the electrochemical performance of batteries.<sup>172–174</sup> For instance, during the drying process, the binder will migrate as the solvent evaporates, resulting in accumulation of the binder on the upper surface of the electrodes.<sup>175</sup> The heterogeneous dispersion of binders gives rise to insufficient adhesion where binders are deficient and electron pathways are hence blocked.<sup>176</sup>

Binders with polar functional groups can improve the affinity and adhesion to hydrophilic interfaces, such as those of silica-based materials. But, at the same time, polar functional groups are also not satisfactory for the dispersion of hydrophobic materials, including various carbonaceous materials, such as graphite and conductive carbon. Amphiphilic binders can promote the dispersion of hydrophilic active materials and hydrophobic carbonaceous constituents simultaneously.<sup>79,100,104</sup> Hu *et al.* designed a triblock copolymer binder, referred to as PESA, consisting of phenyl, alkoxy, and carboxyl groups for silicon/graphite anodes.<sup>100</sup> Among functional groups, the phenyl group has a fair affinity with graphite surfaces *via*  $\pi$ - $\pi$  interactions, while the carboxyl group is attracted to silicon surfaces *via* hydrogen bonding. Moreover, the alkoxy group satisfies the stretchability of polymers (Fig. 8a). As exhibited by the optical photos in Fig. 8b, the water slurry of Si/C components with the PSEA binder is visually dispersed more uniformly (right) compared to CMC/SBR binders that were obviously stratified (left). Peeling-off tests, which were influenced by the homogeneity of each component and the interactive strength between each component and binders, indicate the higher average peeling-off force for PSEA-based electrodes ( $163\text{ N m}^{-1}$ ) compared with CMC/SBR ( $100\text{ N m}^{-1}$ ) and PAA ( $24\text{ N m}^{-1}$ ) (Fig. 8c).

Another example is a renatured DNA (reDNA) skeleton conjugated with alginate segments *via* noncovalent bonds to yield an amphiphilic brush-structure binder.<sup>104</sup> Denaturation upon heat treatment opened up the DNA double helix, while the subsequent renaturation by cooling did not completely restore the base-pair pairing, where the heterocyclic aromatic

moieties were exposed to enhance the interactions with the hydrophobic surfaces of graphite and conductive carbon. In addition, the alginate segments showed a strong affinity with the hydrophilic surfaces of silicon. Optical microscopy images showed less agglomeration on the Si@reDNA/alginate surface than on Si@alginate. Furthermore, the images after peeling-off showed less Cu surface exposure for Si@reDNA/alginate than for Si@reDNA, Si@DNA and Si@alginate, which was attributed to the even adhesion from the homogeneous distribution of each component.

As for electrolyte infiltration inside the electrode, for instance, the electrolyte had a smaller contact angle on a Si electrode with a PAA-DA/PVA binder possessing abundant hydroxyl and carboxyl groups ( $14.6^{\circ}$ ) compared to that for a Si electrode with a CMC/SBR binder ( $23.9^{\circ}$ ), demonstrating that the electrolyte on the surface with a PAA-DA/PVA binder had a larger surface tension and better wettability.<sup>161</sup> The swelling properties of binders can also accelerate electrolyte infiltration through electrolyte uptake. By grafting a flexible and long epoxy chain, the weight change of the binder after swelling due to electrolyte uptake was up to  $468.8\%$  compared to PVDF ( $29.1\%$ ) and CMC ( $24.2\%$ ).<sup>103</sup> A drop of electrolyte disappeared completely on the electrodes with the grafted binders within 3 minutes. In addition, binders with a 3D skeleton-structure can also accelerate electrolyte dispersion due to the large porosity and specific surface area.<sup>84,85,177,178</sup> Wang *et al.* proposed a composite binder consisting of carbon nanotubes interwoven by cellulose to construct a 2D reticular nanosheet structure (named as 3C-binder) (Fig. 8d).<sup>84</sup> The contact angle of the electrolyte on the electrode surface with PVDF was initially  $79^{\circ}$  and was maintained at  $33^{\circ}$  after 30 s. In contrast, the contact angle of the 3C-binder was initially  $55^{\circ}$  and electrolyte permeated through the electrode completely after 5 s, which was attributed to the binder's porous structure (Fig. 8e).

The dispersion of the binders themselves in a solvent depends mainly on the polarity of the solvents and binders. PVDF is generally soluble only in organic solvents with strong polarity, such as NMP, which is however toxic and causes environmental pollution. Water is an ideal green solvent and is hoped to replace NMP in electrode manufacture. Therefore, aqueous binders are widely employed and investigated, such as PAA. Aqueous binders need to have sufficient hydrophilic groups, such as hydroxyl, carboxyl, and amino groups, to ensure water solubility.<sup>179</sup> Bio-polymers and their derivatives are promising candidates, attributed to their water solubility, biodegradability and sustainability, such as CMC and polysaccharides (*e.g.*, alginate).<sup>180,181</sup> A tragacanth gum-based binder was used in lithium-sulfur batteries, which had characteristics of nonflammability, water solubility and environmental compatibility.<sup>74</sup> Based on this binder, the batteries demonstrated superior electrochemical performance.

Plagued by the toxicity of the traditional NMP solvent and the huge energy consumption in the electrode drying process,<sup>182</sup> it is a promising strategy to free the use of solvent and develop the solvent-free electrode preparation



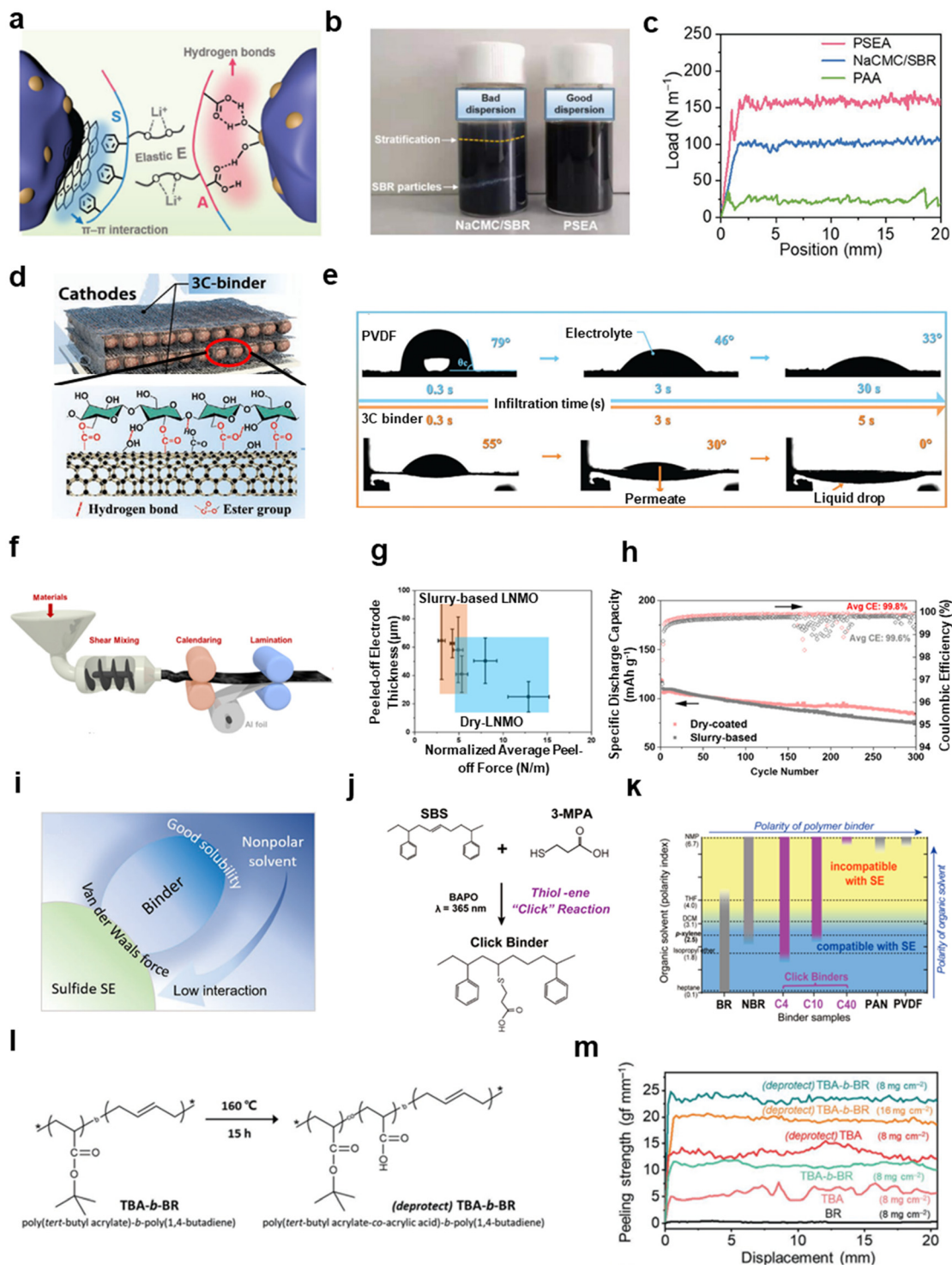


**Fig. 8** Modification strategies to improve the homogeneity of electrodes through functional binders. (a) Schematic illustration of the interaction of the three-block PSEA binder with graphite and silicon in Si/C composite anodes. (b) Photographs of the water slurry of Si/C with CMC/SBR or PSEA. (c) The peeling-off tests of Si/C electrodes with PSEA, CMC/SBR and PAA. (a)–(c) are reproduced with permission.<sup>100</sup> Copyright 2022, Wiley. (d) Schematic diagram of 3C composite binder. (e) The contact angles of electrolyte on electrodes with PVDF or 3C binders at different testing times. (d) and (e) are reproduced with permission.<sup>84</sup> Copyright 2021, Wiley. (f) Schematic diagram of the dry-coating manufacturing process for electrode preparation. (g) The relationship between normalized average peeling-off force and electrode thickness for slurry-based LNMO and dry LNMO electrodes. (h) Cycling performance of slurry-based LNMO and dry LNMO electrodes. (f)–(h) are reproduced with permission.<sup>78</sup> Copyright 2023, Royal Society of Chemistry. (i) Graphical illustration of the compatibility among sulfide electrolyte, binder and solvent. Reproduced with permission.<sup>109</sup> Copyright 2021, Wiley. (j) Schematic illustration of click binder synthesized by thiol-ene click reaction grafting a carboxyl group onto SBS. (k) The solubilities of different binders in various solvents with different polarities, and the compatibility of a sulfide electrolyte with solvents. (j) and (k) are reproduced with permission.<sup>58</sup> Copyright 2019, American Chemical Society. (l) Synthesis method of (deprotect) TBA-b-BR. (m) Peeling-off test of NCM electrodes with the protected and deprotected binders. (l) and (m) are reproduced with permission.<sup>96</sup> Copyright 2020, Wiley.



manufacturing as shown in Fig. 8f.<sup>78</sup> It is a challenge for the binder to disperse uniformly in the electrode without a solvent as a dispersant.<sup>183</sup> PTFE is attracting much attention because it can maintain a viscous flow state under moderate heating and present a stretched fiber-state under a strong shearing force. Therefore, thermal dispersion can be realized as a suitable preparation method of solvent-free electrodes using a hot roll-pressing process or electrostatic spinning process, which have the potential to match current large-scale manufacturing. Yao *et al.* prepared an LNMO cathode with PTFE and carbon fiber for solvent-free manufacturing.<sup>78</sup> The highest thickness of dry electrodes prepared by this method reached 240  $\mu\text{m}$ , and the corresponding mass loading was up to  $\sim 68 \text{ mg cm}^{-2}$ , and the areal capacity was up to  $\sim 9.5 \text{ mA h cm}^{-2}$ . In sharp contrast, when the areal capacity of slurry-based electrodes reached  $6 \text{ mA h cm}^{-2}$ , the thick electrode developed cracks due to the migration of the binder to the surface during drying and the lack of sufficient adhesion. Dry electrodes showed a higher thickness and even better adhesion than the slurry-based electrodes (Fig. 8g). It is inspiring that the cycling performance showed the capacity retention of the dry-coated LNMO full cell was 80% after 300 cycles, while the capacity retention of the slurry-based cell was 67% (Fig. 8h).

In all-solid-state batteries employing sulfide solid electrolytes, weakly polar or nonpolar solvents are often used in the electrode preparation to avoid side reactions with chemically active sulfide electrolyte. However, PVDF cannot be dissolved in nonpolar solvents, which requires binders with reduced polarity to match the solid-electrolyte/electrode preparation process. The decrease of polarity generally leads to insufficient adhesion. Therefore, how to balance the solubility in nonpolar solvents and the adequate adhesion with electrodes needs to be carefully considered (Fig. 8i).<sup>109</sup> SBS polymer, whose polarity was regulated by grafting carboxyl groups through a thiol-ene click reaction (Fig. 8j),<sup>58</sup> exhibited the compatibility of different binders (Fig. 8k, horizontal axis, the polarity increased from left to right) and different organic solvents (Fig. 8k, vertical axis, the dielectric constant increases from bottom to top). It is worth noting that the 2022 Nobel Prize for Chemistry was awarded to click chemistry. The yellow area at the top represents solvents that were too polar to be compatible with the sulfide electrolyte (including NMP, tetrahydrofuran), and the blue area at the bottom represents the solvents that were compatible with the sulfide electrolyte (including dichloromethane, *p*-xylene, isopropyl ether and heptane). C40 (molar ratios of SBS and carboxyl groups at 100 : 4) was not soluble in *p*-xylene and not used in electrode preparation, but lower SBS contents (C4 and C10) were suitable. The aforementioned trade-off in sulfide solid electrolyte can also be overcome by the *in situ* deprotection method proposed by Lee *et al.*<sup>96</sup> A block copolymer of butadiene rubber (BR) with tri-butyl acrylate was synthesized (named as TBA-*b*-BR). The weakly polar ester bond in TBA-*b*-BR, which was beneficial to dissolution in the nonpolar solvent (*i.e.*, butyl butyrate), could be decomposed into a carboxyl

group with stronger polarity by heating at 160 °C. The adhesion was thus enhanced as shown in the peeling-off tests, which demonstrated that deprotected TBA-*b*-BR delivered the highest peeling strength compared to deprotected TBA, TBA-*b*-BR, TBA and BR (Fig. 8l). It clearly demonstrated that this deprotecting strategy enhanced the adhesion of the binders effectively (Fig. 8m). Electrochemical cycling tests showed that batteries with deprotected TBA-*b*-BR delivered superior cyclability in NCM/lithium-indium all-solid-state cells with a capacity retention of 80% for deprotected TBA-*b*-BR, which was higher than for the deprotected TBA and BR with values of 55.7% and 24%, respectively.

### 3 Summary and outlook

Although the binder makes up a rather small proportion of the electrode ( $\sim 5 \text{ wt}\%$ ), it plays a nontrivial role in the battery performance. The fundamental properties of various binders (alkane-based, polysaccharide-based and inorganic classes), including mechanical and thermal properties, are collected in Tables 1, 2, 3 and 4. Typically, the inorganic components of electrodes (active electrode materials, conductive agents, *etc.*) are assembled into a system with structural integrity through the use of flexible polymers (*i.e.*, binders) and maintain a close contact with the current collector. Even though conventional PVDF binders possess decent comprehensive properties in commercial batteries (*e.g.*, LCO/graphite), PVDF is probably no longer suitable for certain high-specific-energy battery systems, such as high-voltage cathodes, silicon anodes, and solid-state-electrolytes (especially sulfide electrolytes). To conclude, the design strategies of functional binders are delineated from the molecular point of view, hopefully to establish the corresponding relationship between binders and special functions of different systems. The corresponding issues and strategies are summarized in Fig. 9. Specifically, (1) binders with high adhesive and mechanical strength are designed to realize the high mass loading of electrode materials *via* stronger interfacial interaction and physical (or chemical) cross-linking; (2) binders with high elasticity or self-healing properties are designed to accommodate volume changes of the electrode through according strategies, such as sacrificial bonds or reversible dynamic bonds; (3) binders are employed to suppress the decomposition of electrolyte on the electrode surface, and construct a stable electrode-electrolyte interface through introducing polar and electron-rich functional groups; (4) the electronic or (5) ionic conductivity of electrodes is improved by designing electronically or ionically conductive binders to realize high-rate charge and discharge utilizing the conjugate polymeric backbone or grafting of flexible fragments; (6) by improving the thermal properties of binders through, for example, using inorganic binders or polyimide-based binders, the thermal safety and wide-temperature operability are enhanced; and (7) the development of binders that provide compatibility with special processes, including aqueous binders, sulfide solid state electrodes and solvent-free electrodes.





## Functional Binders

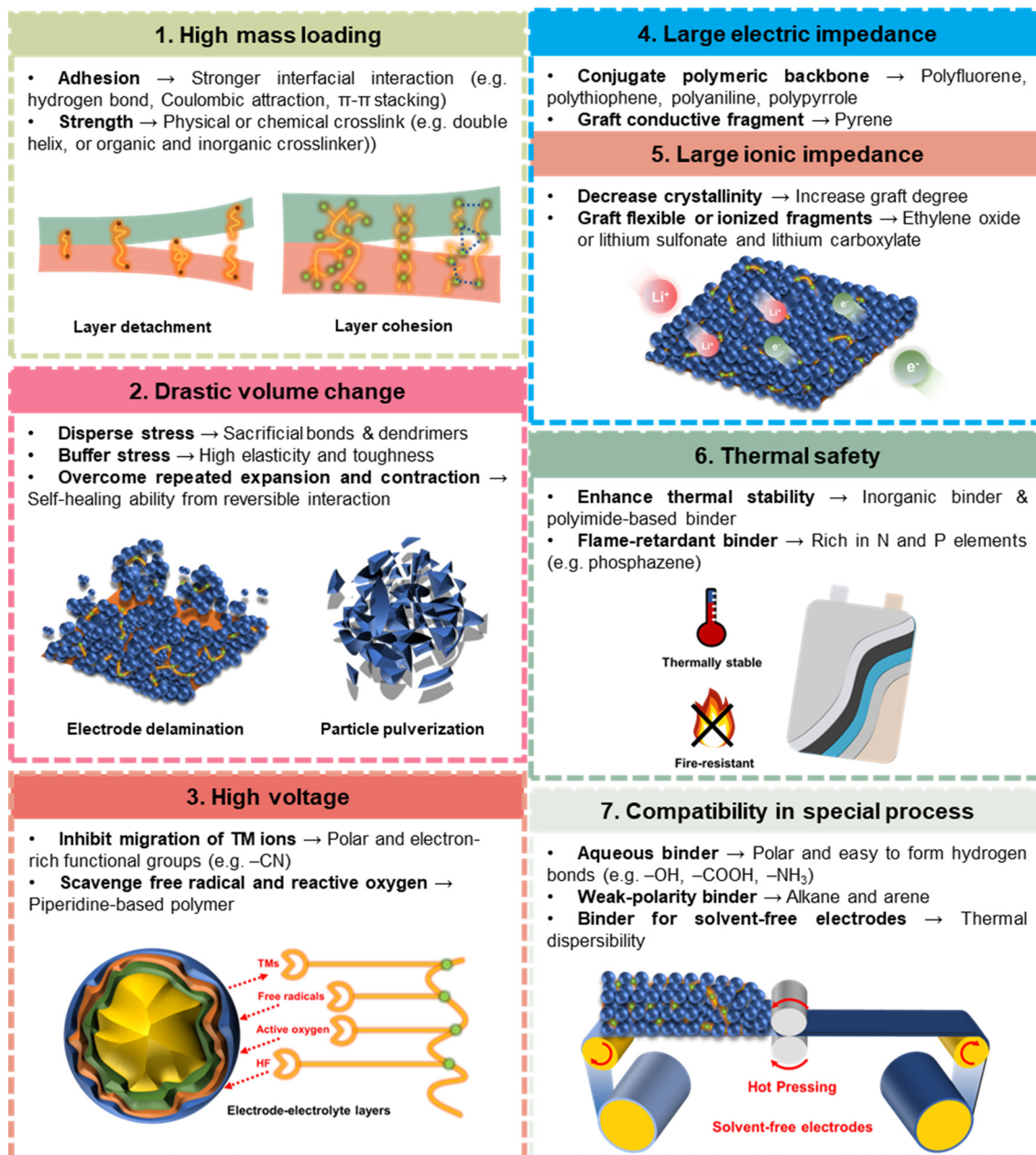
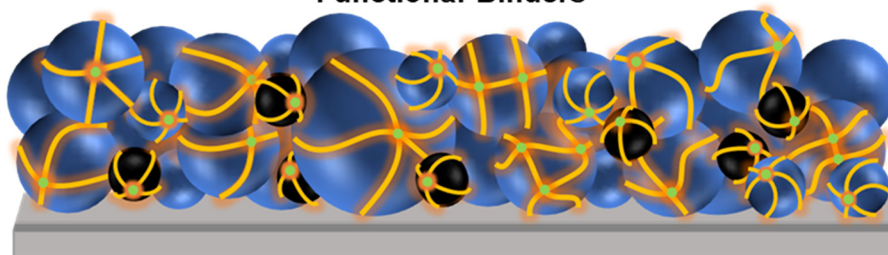


Fig. 9 The seven primary issues and corresponding strategies for functional binders.

Common molecular synthesis strategies for binders include grafting, cross-linking, copolymerization, and blending, which are used to alter the molecular structure of the binders and to endow the binders with different

functions. There is no single binder that realizes all functions and fulfils all requirements, while the most fundamental function is always the adhesion, which means sufficient adhesive and mechanical strength. Another basic function is



the ability of binders to accommodate volume variations, which is particularly important in the system with repeated volume variations. These two functions in the electrodes can only be achieved by binders and are therefore very important. Subsequently, the stability of the binders (chemical, electrochemical and thermal stability) needs to be considered, such as whether it reacts with chemically active species in the electrolytes (*e.g.*, active oxygen, sulfide solid-state electrolyte) or active materials, whether it is electrochemically unstable in the extreme voltage conditions (high voltage or low voltage), and whether the binder fails or is decomposed at extreme temperatures. Finally, certain specialized features brought by the binder are worthy of consideration, such as interface protection, electronic and ionic conductivity, thermal safety and wide temperature operation capability, and improvements in the homogeneity of each component. Because there are other components that are mainly responsible for these features, they are the last to be implemented in a binder. Anyhow, such featured binders can synergistically improve these properties and have a significant effect on the battery performance. Herein, the electrochemical performance results of various binders used in cathodes and anodes are listed in Tables 5 and 6.

Despite the remarkable achievements made in binder design, there are still many challenges to overcome in terms of the following well-recognized rationale:<sup>8,133,188–190</sup> (1) new perspectives and methods for binder molecular design. The correspondences between binder molecular structures and battery performance are still complex. How binder molecular structures affect the binders' properties and further affect the electrodes' properties, as well as finally change the batteries' performance, is far from clear.<sup>62,191</sup> In fact, 'Artificial Intelligence for Science', a recently developed concept, is accelerating the exploration for the material science that utilizes advanced machine learning and deep learning technology, to shed light on the complicated structure–property relationships.<sup>192–195</sup> For example, Zahrt *et al.* recognized the agnostic structural patterns of a chiral catalyst through large datasets and predicted the asymmetric selectivity

quantitatively.<sup>195</sup> We believe the same strategy and workflow can be migrated into binder molecular design. (2) The mechanistic study of binders including characterizations and simulations. The *in situ* characterization and analysis of binders inside the electrodes is extremely difficult due to the low content, the small size and the light elements of the binders.<sup>196</sup> The lack of characterization of the binder distribution in the electrodes as well as the change of binders during battery processing and operation actually impede our understanding of the aging and failure mechanisms from the view of the binders.<sup>175,197,198</sup> Fortunately, several advanced characterization techniques have been employed in the studies of binders, such as acoustic measurements,<sup>199</sup> electrochemical quartz-crystal microbalance,<sup>200</sup> Raman spectrometry,<sup>201</sup> X-ray computed tomography,<sup>197</sup> and so on. For example, scanning transmission electron microscopy and valence energy-loss spectroscopy technologies can be utilized to visualize the distribution of binders on the silicon particle surface.<sup>202</sup> At the same time, simulation methods towards the binder-containing composite electrodes are also developed to reflect the influence of the binder on the batteries.<sup>203</sup> Lombardo *et al.* developed a physics-based three-dimensional model to mimic binder migration during drying and unlock the origin of heterogeneous electrode mesostructures.<sup>204</sup> (3) The functional binders suitable for specific electrode systems. As we mentioned above, based on the requirements of high energy density (*e.g.*, high mass loading and high discharge voltage), high power density (*e.g.*, charge and discharge rate) and high safety (*e.g.*, flame retardants), novel functional binders are needed to replace PVDF. Taking the high-specific-energy electrode systems (the cathodes with LRMO or NCM811 and the anodes with silicon or lithium) as an example, determining whether there is a binder better than PVDF in the aspects of electrochemical performance, economy, and compatibility with manufacturing needs further exploration. (4) Functional binders suitable for new manufacturing. For example, the development of solvent-free manufacturing for electrode fabrication can eliminate the processes of solvent evaporation and recycling, which is beneficial to reduce the cost and improve the efficiency.<sup>205,206</sup>

**Table 5** The electrochemical performance of the binders used in cathodes

| Binders           | Cathode materials                                      | Maximal voltage (V) | Maximal mass loading (mg cm <sup>-2</sup> ) | Maximal rate (C) | Cycles | Capacity retention (%) | Reference |
|-------------------|--|---------------------|---|------------------|--------|------------------------|-----------|
| CMC-CNT           | LCO  | 4.3                 | 86  | ~2               | 350    | 93                     | 84        |
| DSL               | LCO  | 4.6                 | 5   | 0.5              | 100    | 93.4                   | 22        |
| Si-based binder   | LCO  | 4.5                 | 8   | 6                | 100    | 92                     | 184       |
| Anti-aging binder | LCO  | 4.5                 | 5   | 10               | 160    | 97                     | 72        |
| DPGP-PEI/PVDF     | NCM811   | 4.5                 | 2   | 5                | 1000   | 80                     | 51        |
| Anti-aging binder | NCM811   | 4.5                 | 15  | 10               | 100    | 95                     | 72        |
| PANI              | LiNi <sub>0.94</sub> Co <sub>0.06</sub> O <sub>2</sub> | 4.4                 | 8   | 10               | 1000   | 81                     | 132       |
| PNB-g-PAA         | NCM811   | 4.2                 | 27  | 3                | 240    | 80                     | 19        |
| SA-PProDOT        | LFP  | 4.2                 | —   | 2                | 400    | 86.6                   | 185       |
| Lignin            | LNMO   | 5                   | 1.8   | 1                | 1000   | 94.1                   | 186       |
| LiPAA             | LNMO   | 5                   | —   | 20               | 80     | 90                     | 25        |
| Anti-aging binder | LRMO   | 4.7                 | 4   | 10               | 100    | 92                     | 72        |
| PANI              | LRMO   | 4.8                 | —   | 3.3              | 300    | 93                     | 23        |
| FPI               | LRMO   | 4.7                 | 3   | 0.2              | 100    | 89                     | 24        |



**Table 6** The electrochemical performance of the binders used in anodes

| Binders           | Anode materials | Maximal mass loading (mg cm <sup>-2</sup> ) | Maximal rate (C) | Initial coulombic efficiency (%) | Cycles | Capacity retention (%) | Reference |
|-------------------|-----------------|---|------------------|----------------------------------|--------|------------------------|-----------|
| Native-XG         | SiNP            | 1   | 12               | 76                               | 200    | 72.2                   | 82        |
| 3F1V              | SiNP            | 4.9   | 0.2              | 79.9                             | 100    | 66.7                   | 87        |
| N-P-LiPN          | SiNP            | 28.88                                       | 2                | 90.76                            | 100    | 59                     | 28        |
| GG-g-PAM          | SiNP            | 2.3   | ~2               | 87.6                             | 100    | 83.9                   | 75        |
| PTBR              | SiMP            | 5.07  | 0.7              | 89.45                            | 200    | 92                     | 114       |
| PR-PAA            | SiMP            | 1   | 0.4              | 91.22                            | 150    | 91                     | 26        |
| SHP-PEG2000(40)   | SiMP            | 0.7   | 2                | 83                               | 150    | 80                     | 123       |
| PAA-P(HEA-co-DMA) | SiMP            | 1   | ~1.2             | 89.3                             | 220    | 93.8                   | 30        |
| PSEA              | Si/C            | 5   | 2                | 85.1                             | 120    | 92                     | 100       |
| PAHT              | Si/C            | 6   | 0.1              | 90                               | 100    | 89                     | 187       |
| PR-PAA            | Si/C            | 2.5   | 2                | 75.52                            | 250    | 92.6                   | 31        |
| PN-4              | SiO             | 14  | 0.3              | 84                               | 500    | 81.5                   | 38        |
| HOS-PFM           | SiO             | 2.45  | 2                | 69.9                             | 300    | 86.3                   | 32        |
| PAA-P(HEA-co-DMA) | SiO             | 6   | 10               | 70                               | 300    | ~100                   | 30        |

Meanwhile, this process that is free of NMP is environmentally friendly and decreases carbon emissions. However, the compatibility of the binders with the hot-press process needs further investigation and the manufacturing conditions need to be optimized.<sup>86,159</sup> To sum up, further efforts are needed to understand and develop novel functional binders for the next-generation of high-specific-energy batteries. It is believed that, by means of binder design engineering, a bright future will be witnessed for high-specific-energy LIBs.

## Acronyms and abbreviations

|                    |  |                    |   |
|--------------------|--|--------------------|---|
| PVDF               | Polyvinylidene difluoride  | FA                 | Formic acid   |
| CMC/Na-CMC         | Sodium carboxymethylcellulose  | PPy                | Polypyrrole   |
| PAA                | Poly(acrylic acid)   | $T_g$              | Glass transition temperature  |
| SBR                | Styrene-butadiene rubber   | $T_f$              | Viscous flow temperature  |
| XG                 | Xanthan gum  | $T_d$              | Decomposition temperature   |
| GG                 | Guar gum   | CB                 | Carbon black  |
| TG                 | Tragacanth gum   | SEM                | Scanning electron microscope  |
| TM                 | Transition metal   | LIB                | Lithium-ion battery   |
| CEI                | Cathode electrolyte interphase   | CNT                | Carbon nanotube   |
| SEI                | Solid electrolyte interphase   | SOC                | State of charge   |
| PANI               | Polyaniline  | DEMS               | Differential electrochemical mass spectrometry  |
| PEI                | Polyethylenimine   | HAADF-STEM         | High-angle annular dark-field scanning transmission electron microscopy   |
| LRMO               | Li-rich Mn-based oxide ( $x\text{Li}_2\text{MnO}_3 \cdot (1-x)\text{LiMO}_2$ (M = Mn, Ni, Co)) | XPS                | X-ray photoelectron spectroscopy  |
| LCO                | Lithium cobalt oxide ( $\text{LiCoO}_2$ )  | EIS                | Electrochemical impedance spectroscopy  |
| NCM811             | Ni-rich layered oxide cathode ( $\text{LiNi}_{0.8}\text{Co}_{0.1}\text{Mn}_{0.1}\text{O}_2$ )  | DSC                | Differential scanning calorimetry   |
| LFP                | Lithium iron phosphate ( $\text{LiFePO}_4$ )   | TOF-SIMS           | Time-of-flight secondary ion mass spectrometry  |
| LNMO               | $\text{LiNi}_{0.5}\text{Mn}_{1.5}\text{O}_4$   | Ph                 | Phenyl  |
| LMO                | $\text{LiMn}_2\text{O}_4$  | SHP                | Self-healing polymer  |
| PAN                | Polyacrylonitrile  | N-P-LiPN           | Partially lithiated polyacrylic acid and Nafion   |
| LUMO               | Lower unoccupied molecular orbital   | P-LiPAA            | Partially lithiated polyacrylic acid  |
| m-SiO <sub>x</sub> | Microparticle SiO <sub>x</sub>   | P-LiNF             | Partially lithiated Nafion  |
| SiMP               | Microparticle silicon  | PAA-P (HEA-co-DMA) | poly(acrylic acid)-poly(2-hydroxyethyl acrylate-co-dopamine methacrylate)   |
| SiNP               | Nanoparticle silicon   | DPGP               | Catechol grafted poly(glycidyl methacrylate-co-pentafluorophenyl acrylate-co-poly(ethylene glycol) methyl ether methacrylate) |
| PEDOT:PSS          | Poly(3,4-ethylene dioxythiophene) doped with poly(styrene sulfonate)                           | PR-PAA             | Polyrotaxane-poly(acrylic acid)   |
|                    |  | UCFR               | Ultrahigh-capacity, fire-resistant binders  |
|                    |  | HOS                | Hierarchically ordered structures   |
|                    |  | HPF                | Poly(9,9-dioctylfluorene-co-(9H-fluorene))  |





|            |   |
|------------|---|
| PF         | Poly(9,9dioctylfluorene- <i>co</i> -fluorenone)   |
| PFM        | Poly(9,9-dioctylfluorene- <i>co</i> -fluorenone- <i>co</i> -methylbenzoic ester)  |
| PEFM       | Poly(9,9-di(oxy-2,5,8-trioxadecane)fluorene- <i>co</i> -(9,9-dioctylfluorene)- <i>co</i> -methylbenzoic ester)                  |
| Mn-COP     | Mn-covalent-bonding organic polymer   |
| xFyV       | x poly (furfuryl alcohol):y polyvinyl alcohol (x, y = 1, 2, 3)  |
| PFA        | Poly (furfuryl alcohol)   |
| PVA        | Polyvinyl alcohol   |
| PAM        | Polyacrylamide  |
| Cx         | Molar ratios of SBS and carboxyl groups at 100:x in binders (x = 4, 10, 40)   |
| APP        | Ammonium polyphosphate  |
| TrFE       | Trifluoroethylene   |
| SPS        | Sulfonated poly(styrene)  |
| BR         | Butadiene rubber  |
| TBA        | Tri-butyl acrylate  |
| ECH        | Epichlorohydrin   |
| PG         | Peach gum   |
| Alg-C      | Catechol-grafted alginate   |
| PAA-C      | Catechol-grafted PAA  |
| XNBR       | Carboxyl nitrile rubber   |
| TA         | Tannic acid   |
| PTBR       | PAA-TA-XNBR   |
| β-CDP      | β-Cyclodextrin polymers   |
| PEG        | Polyethylene glycol   |
| AD         | Adamantane  |
| GA         | Gallol  |
| HA         | Hyaluronic acid   |
| PS         | Photostabilizer   |
| DSL        | Dextran sulfate lithium   |
| PVAm       | Poly(vinylamine)  |
| TEGDA      | Tetra(ethylene glycol) diacrylate   |
| BBP        | Bottlebrush polymer   |
| PI-FTD     | Fluorinated polyimide   |
| EP         | Eugenol phosphazene   |
| HAP        | Hydroxyapatite nanowires  |
| reDNA      | Renatured DNA   |
| PNB        | Polynorborene   |
| SA-PProDOT | Sodium alginate-poly(3,4-propylenedioxythiophene-2,5-dicarboxylic acid)   |
| FPI        | Fluorinated polyimide   |
| PSEA       | Triblock binders composed of polystyrene (S), poly(2-(2-methoxyethoxy) ethyl acrylate) (E), and poly(acrylic acid) (A) segments |
| PAHT       | Binders incorporating tannic acid to poly(acrylic acid- <i>co</i> -2-hydroxyethyl acrylate)                                     |
| PN-4       | Positively and negatively charged binders   |

## Conflicts of interest

The authors declare no conflict of interest.

## Acknowledgements

The authors are grateful for funding support from National Natural Science Foundation of China (grant no. 52325207, 22239003) and CAS Project for Young Scientists in Basic Research (Grant No. YSBR-058).

## References

- 1 Y. Liu, Y. Zhu and Y. Cui, Challenges and opportunities towards fast-charging battery materials, *Nat. Energy*, 2019, **4**, 540–550.
- 2 J. M. Tarascon and M. Armand, Issues and challenges facing rechargeable lithium batteries, *Nature*, 2001, **414**, 359–367.
- 3 M. Armand and J. M. Tarascon, Building better batteries, *Nature*, 2008, **451**, 652–657.
- 4 C. Wang, C. Yang and Z. Zheng, Toward practical high-energy and high-power lithium battery anodes: Present and future, *Adv. Sci.*, 2022, **9**, 2105213.
- 5 Q. Cheng, Z.-X. Chen, X.-Y. Li, L.-P. Hou, C.-X. Bi, X.-Q. Zhang, J.-Q. Huang and B.-Q. Li, Constructing a 700 Wh kg<sup>-1</sup> level rechargeable lithium-sulfur pouch cell, *J. Energy Chem.*, 2023, **76**, 181–186.
- 6 Q. Li, Y. Yang, X. Yu and H. Li, A 700 W-h-kg<sup>-1</sup> rechargeable pouch type lithium battery, *Chin. Phys. Lett.*, 2023, **40**, 048201.
- 7 X. Ma, J. Yu, Y. Hu, J. Texter and F. Yan, Ionic liquid/poly(ionic liquid)-based electrolytes for lithium batteries, *Ind. Chem. Mater.*, 2023, **1**, 39–59.
- 8 H. Chen, M. Ling, L. Hencz, H. Y. Ling, G. R. Li, Z. Lin, G. Liu and S. Q. Zhang, Exploring chemical, mechanical, and electrical functionalities of binders for advanced energy-storage devices, *Chem. Rev.*, 2018, **118**, 8936–8982.
- 9 T. W. Kwon, J. W. Choi and A. Coskun, The emerging era of supramolecular polymeric binders in silicon anodes, *Chem. Soc. Rev.*, 2018, **47**, 2145–2164.
- 10 T.-w. Kwon, J. W. Choi and A. Coskun, Prospect for supramolecular chemistry in high-energy-density rechargeable batteries, *Joule*, 2019, **3**, 662–682.
- 11 Y. Zhao, Z. Liang, Y. Kang, Y. Zhou, Y. Li, X. He, L. Wang, W. Mai, X. Wang, G. Zhou, J. Wang, J. Li, N. Tavajohi and B. Li, Rational design of functional binder systems for high-energy lithium-based rechargeable batteries, *Energy Storage Mater.*, 2021, **35**, 353–377.
- 12 Y. Ma, J. Ma and G. Cui, Small things make big deal: Powerful binders of lithium batteries and post-lithium batteries, *Energy Storage Mater.*, 2019, **20**, 146–175.
- 13 F. Zou and A. Manthiram, A review of the design of advanced binders for high-performance batteries, *Adv. Energy Mater.*, 2020, **10**, 2002508.
- 14 W. Xia and Z. Zhang, PVDF-based dielectric polymers and their applications in electronic materials, *IET Nanodielectrics*, 2018, **1**, 17–31.



- 15 Q. Jia, Q. Li, M. Luo and H.-B. Li, Understanding the effects of vicinal carbon substituents and configuration on organofluorine hydrogen-bonding interaction, *RSC Adv.*, 2018, **8**, 38980–38986.
- 16 Y. Wu, Y. Li, Y. Wang, Q. Liu, Q. Chen and M. Chen, Advances and prospects of PVDF based polymer electrolytes, *J. Energy Chem.*, 2022, **64**, 62–84.
- 17 V. F. Cardoso, D. M. Correia, C. Ribeiro, M. M. Fernandes and S. Lanceros-Méndez, Fluorinated polymers as smart materials for advanced biomedical applications, *Polymers*, 2018, **10**, 161.
- 18 J. E. Marshall, A. Zhenova, S. Roberts, T. Petchey, P. Zhu, C. E. J. Dancer, C. R. McElroy, E. Kendrick and V. Goodship, On the solubility and stability of polyvinylidene fluoride, *Polymers*, 2021, **13**, 1354.
- 19 N.-Y. Kim, J. Moon, M.-H. Ryou, S.-H. Kim, J.-H. Kim, J.-M. Kim, J. Bang and S.-Y. Lee, Amphiphilic bottlebrush polymeric binders for high-mass-loading cathodes in lithium-ion batteries, *Adv. Energy Mater.*, 2022, **12**, 2102109.
- 20 Y. H. Kwon, K. Minnici, M. M. Huie, K. J. Takeuchi, E. S. Takeuchi, A. C. Marschilok and E. Reichmanis, Electron/Ion transport enhancer in high capacity li-ion battery anodes, *Chem. Mater.*, 2016, **28**, 6689–6697.
- 21 S. Radloff, R. G. Scurtu, M. Hölzle and M. Wohlfahrt-Mehrens, Water-based  $\text{LiNi}_{0.83}\text{Co}_{0.12}\text{Mn}_{0.05}\text{O}_2$  electrodes with excellent cycling stability fabricated using unconventional binders, *J. Electrochem. Soc.*, 2022, **169**, 040514.
- 22 H. Huang, Z. Li, S. Gu, J. Bian, Y. Li, J. Chen, K. Liao, Q. Gan, Y. Wang, S. Wu, Z. Wang, W. Luo, R. Hao, Z. Wang, G. Wang and Z. Lu, Dextran sulfate lithium as versatile binder to stabilize high-voltage  $\text{LiCoO}_2$  to 4.6 V, *Adv. Energy Mater.*, 2021, **11**, 2101864.
- 23 Z. Xu, X. Guo, J. Wang, Y. Yuan, Q. Sun, R. Tian, H. Yang and J. Lu, Restraining the octahedron collapse in lithium and manganese rich NCM cathode toward suppressing structure transformation, *Adv. Energy Mater.*, 2022, **12**, 2201323.
- 24 H. Q. Pham, G. Kim, H. M. Jung and S.-W. Song, Fluorinated polyimide as a novel high-voltage binder for high-capacity cathode of lithium-ion batteries, *Adv. Funct. Mater.*, 2018, **28**, 1704690.
- 25 N. P. W. Pieczonka, V. Borgel, B. Ziv, N. Leifer, V. Dargel, D. Aurbach, J.-H. Kim, Z. Liu, X. Huang, S. A. Krachkovskiy, G. R. Goward, I. Halalay, B. R. Powell and A. Manthiram, Lithium polyacrylate (LiPAA) as an advanced binder and a passivating agent for high-voltage Li-ion batteries, *Adv. Energy Mater.*, 2015, **5**, 1501008.
- 26 S. Choi, T. W. Kwon, A. Coskun and J. W. Choi, Highly elastic binders integrating polyrotaxanes for silicon microparticle anodes in lithium ion batteries, *Science*, 2017, **357**, 279–283.
- 27 T.-w. Kwon, Y. K. Jeong, E. Deniz, S. Y. AlQaradawi, J. W. Choi and A. Coskun, Dynamic cross-linking of polymeric binders based on host-guest interactions for silicon anodes in lithium ion batteries, *ACS Nano*, 2015, **9**, 11317–11324.
- 28 Z. H. Li, Y. P. Zhang, T. F. Liu, X. H. Gao, S. Y. Li, M. Ling, C. D. Liang, J. C. Zheng and Z. Lin, Silicon anode with high initial Coulombic Efficiency by modulated trifunctional binder for high-areal-capacity lithium-ion batteries, *Adv. Energy Mater.*, 2020, **10**, 1903110.
- 29 M. H. Ryou, J. Kim, I. Lee, S. Kim, Y. K. Jeong, S. Hong, J. H. Ryu, T. S. Kim, J. K. Park, H. Lee and J. W. Choi, Mussel-inspired adhesive binders for high-performance silicon nanoparticle anodes in lithium-ion batteries, *Adv. Mater.*, 2013, **25**, 1571–1576.
- 30 Z. Xu, J. Yang, T. Zhang, Y. Nuli, J. Wang and S.-i. Hirano, Silicon microparticle anodes with self-healing multiple network binder, *Joule*, 2018, **2**, 950–961.
- 31 Y. Cho, J. Kim, A. Elabd, S. Choi, K. Park, T.-w. Kwon, J. Lee, K. Char, A. Coskun and J. W. Choi, A pyrene-poly(acrylic acid)-polyrotaxane supramolecular binder network for high-performance silicon negative electrodes, *Adv. Mater.*, 2019, **31**, 1905048.
- 32 T. Zhu, H. Sternlicht, Y. Ha, C. Fang, D. Liu, B. H. H. Savitzky, X. Zhao, Y. Lu, Y. Fu, C. Ophus, C. Zhu, W. Yang, A. M. M. Minor and G. Liu, Formation of hierarchically ordered structures in conductive polymers to enhance the performances of lithium-ion batteries, *Nat. Energy*, 2023, **8**, 129–137.
- 33 G. Jiang, K. Li, F. Yu, X. Li, J. Mao, W. Jiang, F. Sun, B. Dai and Y. Li, Robust artificial solid-electrolyte interfaces with biomimetic ionic channels for dendrite-free Li metal anodes, *Adv. Energy Mater.*, 2021, **11**, 2003496.
- 34 Y. Liu, D. Lin, P. Y. Yuen, K. Liu, J. Xie, R. H. Dauskardt and Y. Cui, An artificial solid electrolyte interphase with high Li-ion conductivity, mechanical strength, and flexibility for stable lithium metal anodes, *Adv. Mater.*, 2017, **29**, 1605531.
- 35 Y. Ren, Z. Cui, A. Bhargav, J. He and A. Manthiram, A self-healable sulfide/polymer composite electrolyte for long-life, low-lithium-excess lithium-metal batteries, *Adv. Funct. Mater.*, 2022, **32**, 2106680.
- 36 W. Ji, H. Qu, X. Zhang, D. Zheng and D. Qu, Electrode architecture design to promote charge-transport kinetics in high-loading and high-energy lithium-based batteries, *Small Methods*, 2021, **5**, 2100518.
- 37 Y. Z. Lai, H. Y. Li, Q. Yang, H. D. Li, Y. X. Liu, Y. Song, Y. J. Zhong, B. H. Zhong, Z. G. Wu and X. D. Guo, Revisit the progress of binders for a silicon-based anode from the perspective of designed binder structure and special sized silicon nanoparticles, *Ind. Eng. Chem. Res.*, 2022, **61**, 6246–6268.
- 38 D.-Y. Han, I. K. Han, H. B. Son, Y. S. Kim, J. Ryu and S. Park, Layering charged polymers enable highly integrated high-capacity battery anodes, *Adv. Funct. Mater.*, 2023, **33**, 2370102.
- 39 J.-M. Kim, J. A. Kim, S.-H. Kim, I. S. Uhm, S. J. Kang, G. Kim, S.-Y. Lee, S.-H. Yeon and S.-Y. Lee, All-nanomat lithium-ion batteries: A new cell architecture platform for ultrahigh energy density and mechanical flexibility, *Adv. Energy Mater.*, 2017, **7**, 1701099.



- 40 J.-M. Kim, C.-H. Park, Q. Wu and S.-Y. Lee, 1D building blocks-intermingled heteronanomats as a platform architecture for high-performance ultrahigh-capacity lithium-ion battery cathodes, *Adv. Energy Mater.*, 2016, **6**, 1501594.
- 41 C. Li, Q. Sun, Q. Zhang, C. Xu, S. Wang, Y. Ma, X. Shi, H. Zhang, D. Song and L. Zhang, Multifunctional binder capable of promoting the reaction dynamics of wide temperature operable lithium-sulfur battery, *Chem. Eng. J.*, 2023, **455**, 140706.
- 42 S. Jiao, Q. Li, X. Xiong, X. Yu, H. Li, L. Chen and X. Huang, Achieving high-energy-density lithium-ion batteries through oxygen redox of cathode: From fundamentals to applications, *Appl. Phys. Lett.*, 2022, **121**, 070501.
- 43 J. Oh, S. H. Choi, B. Chang, J. Lee, T. Lee, N. Lee, H. Kim, Y. Kim, G. Im, S. Lee and J. W. Choi, Elastic binder for high-performance sulfide-based all-solid-state batteries, *ACS Energy Lett.*, 2022, **7**, 1374–1382.
- 44 X. Yao, C. Guo, C. Song, M. Lu, Y. Zhang, J. Zhou, H.-M. Ding, Y. Chen, S.-L. Li and Y.-Q. Lan, In situ interweaved high sulfur loading Li-S cathode by catalytically active metalloporphyrin based organic polymer binders, *Adv. Mater.*, 2023, **35**, 2208846.
- 45 Y. Zhang, A. Hu, D. Xia, S. Hwang, S. Sainio, D. Nordlund, F. M. Michel, R. B. Moore, L. Li and F. Lin, Operando characterization and regulation of metal dissolution and redeposition dynamics near battery electrode surface, *Nat. Nanotechnol.*, 2023, **18**, 790–797.
- 46 J. Wandt, A. T. S. Freiberg, A. Ogrodnik and H. A. Gasteiger, Singlet oxygen evolution from layered transition metal oxide cathode materials and its implications for lithium-ion batteries, *Mater. Today*, 2018, **21**, 825–833.
- 47 T. T. Dong, P. Z. Mu, S. Zhang, H. R. Zhang, W. Liu and G. L. Cui, How do polymer binders assist transition metal oxide cathodes to address the challenge of high-voltage lithium battery applications?, *Electrochem. Energy Rev.*, 2021, **4**, 545–565.
- 48 J. Yang, P. Li, F. Zhong, X. Feng, W. Chen, X. Ai, H. Yang, D. Xia and Y. Cao, Suppressing voltage fading of Li-rich oxide cathode via building a well-protected and partially-protonated surface by polyacrylic acid binder for cycle-stable Li-ion batteries, *Adv. Energy Mater.*, 2020, **10**, 1904264.
- 49 A. Guéguen, D. Streich, M. He, M. Mendez, F. F. Chesneau, P. Novák and E. J. Berg, Decomposition of LiPF<sub>6</sub> in high energy lithium-ion batteries studied with online electrochemical mass spectrometry, *J. Electrochem. Soc.*, 2016, **163**, A1095.
- 50 C. C. Nguyen, T. Yoon, D. M. Seo, P. Guduru and B. L. Lucht, Systematic investigation of binders for silicon anodes: Interactions of binder with silicon particles and electrolytes and effects of binders on solid electrolyte interphase formation, *ACS Appl. Mater. Interfaces*, 2016, **8**, 12211–12220.
- 51 B. Jin, Z. Cui and A. Manthiram, In situ interweaved binder framework mitigating the structural and interphasial degradations of high-nickel cathodes in lithium-ion batteries, *Angew. Chem., Int. Ed.*, 2023, **62**, e202301241.
- 52 L. Gan, R. Chen, X. Yu and H. Li, Understanding the battery safety improvement enabled by a quasi-solid-state battery design, *Chin. Phys. B*, 2022, **31**, 118202.
- 53 R. Chen, Q. Li, X. Yu, L. Chen and H. Li, Approaching practically accessible solid-state batteries: stability issues related to solid electrolytes and interfaces, *Chem. Rev.*, 2020, **120**, 6820–6877.
- 54 L. Trahey, F. R. Brushett, N. P. Balsara, G. Ceder, L. Cheng, Y. M. Chiang, N. T. Hahn, B. J. Ingram, S. D. Minteer, J. S. Moore, K. T. Mueller, L. F. Nazar, K. A. Persson, D. J. Siegel, K. Xu, K. R. Zavadil, V. Srinivasan and G. W. Crabtree, Energy storage emerging: A perspective from the Joint Center for Energy Storage Research, *Proc. Natl. Acad. Sci. U. S. A.*, 2020, **117**, 12550–12557.
- 55 D. A. Gribble, E. McCulfor, Z. Li, M. Parekh and V. G. Pol, Enhanced capacity and thermal safety of lithium-ion battery graphite anodes with conductive binder, *J. Power Sources*, 2023, **553**, 232204.
- 56 B. Koo, H. Kim, Y. Cho, K. T. Lee, N. S. Choi and J. Cho, A highly cross-linked polymeric binder for high-performance silicon negative electrodes in lithium ion batteries, *Angew. Chem., Int. Ed.*, 2012, **51**, 8762–8767.
- 57 Y. Nikodimos, C.-J. Huang, B. W. Taklu, W.-N. Su and B. J. Hwang, Chemical stability of sulfide solid-state electrolytes: Stability toward humid air and compatibility with solvents and binders, *Energy Environ. Sci.*, 2022, **15**, 991–1033.
- 58 K. Lee, J. Lee, S. Choi, K. Char and J. W. Choi, Thiol-Ene Click Reaction for fine polarity tuning of polymeric binders in solution-processed all-solid-state batteries, *ACS Energy Lett.*, 2019, **4**, 94–101.
- 59 J. W. Cho and H. Y. Song, Dehydrofluorination of a copolymer of vinylidene fluoride and tetrafluoroethylene by phase transfer catalysis reaction, *J. Polym. Sci., Part A: Polym. Chem.*, 1995, **33**, 2109–2112.
- 60 C. Bolli, A. Gueguen, M. A. Mendez and E. J. Berg, Operando monitoring of F<sup>-</sup> formation in lithium ion batteries, *Chem. Mater.*, 2019, **31**, 1258–1267.
- 61 S. S. Zhang, X. Fan and C. Wang, Enhanced electrochemical performance of Ni-rich layered cathode materials by using LiPF<sub>6</sub> as a cathode additive, *ChemElectroChem*, 2019, **6**, 1536–1541.
- 62 H. L. Wang, B. Z. Wu, X. K. Wu, Q. Q. Zhuang, T. Liu, Y. Pan, G. J. Shi, H. M. Yi, P. Xu, Z. N. Xiong, S. L. Chou and B. F. Wang, Key factors for binders to enhance the electrochemical performance of silicon anodes through molecular design, *Small*, 2022, **18**, 2101680.
- 63 A. Oishi, R. Tatara, E. Togo, H. Inoue, S. Yasuno and S. Komaba, Sulfated alginate as an effective polymer binder for high-voltage LiNi<sub>0.5</sub>Mn<sub>1.5</sub>O<sub>4</sub> electrodes in lithium-ion batteries, *ACS Appl. Mater. Interfaces*, 2022, **14**, 51808–51818.
- 64 L. Wei, C. Chen, Z. Hou and H. Wei, Poly (acrylic acid sodium) grafted carboxymethyl cellulose as a high performance polymer binder for silicon anode in lithium ion batteries, *Sci. Rep.*, 2016, **6**, 19583.





- 65 G. L. Gregory, H. Gao, B. Liu, X. Gao, G. J. Rees, M. Pasta, P. G. Bruce and C. K. Williams, Buffering volume change in solid-state battery composite cathodes with CO<sub>2</sub>-derived block polycarbonate ethers, *J. Am. Chem. Soc.*, 2022, **144**, 17477–17486.
- 66 J. Liu, D. G. D. Galpaya, L. J. Yan, M. H. Sun, Z. Lin, C. Yan, C. D. Liang and S. Q. Zhang, Exploiting a robust biopolymer network binder for an ultrahigh-areal-capacity Li-S battery, *Energy Environ. Sci.*, 2017, **10**, 750–755.
- 67 I. Kovalenko, B. Zdyrko, A. Magasinski, B. Hertzberg, Z. Milicev, R. Burtovyy, I. Luzinov and G. Yushin, A major constituent of brown algae for use in high-capacity Li-ion batteries, *Science*, 2011, **334**, 75–79.
- 68 P. Parikh, M. Sina, A. Banerjee, X. Wang, M. S. D'Souza, J.-M. Dour, E. A. Wu, O. Y. Trieu, Y. Gong, Q. Zhou, K. Snyder and Y. S. Meng, Role of polyacrylic acid (PAA) binder on the solid electrolyte interphase in silicon anodes, *Chem. Mater.*, 2019, **31**, 2535–2544.
- 69 I. Dueramae, M. Okhawilai, P. Kasemsiri, H. Uyama and R. Kita, Properties enhancement of carboxymethyl cellulose with thermo-responsive polymer as solid polymer electrolyte for zinc ion battery, *Sci. Rep.*, 2020, **10**, 12587.
- 70 A. Abdel-Hakim, T. M. El-Basheer and A. Abdelkhalik, Mechanical, acoustical and flammability properties of SBR and SBR-PU foam layered structure, *Polym. Test.*, 2020, **88**, 106536.
- 71 S. Gao, F. Sun, N. Liu, H. Yang and P.-F. Cao, Ionic conductive polymers as artificial solid electrolyte interphase films in Li metal batteries – A review, *Mater. Today*, 2020, **40**, 140–159.
- 72 P. Mu, H. Zhang, H. Jiang, T. Dong, S. Zhang, C. Wang, J. Li, Y. Ma, S. Dong and G. Cui, Bioinspired antiaging binder additive addressing the challenge of chemical degradation of electrolyte at cathode/electrolyte interphase, *J. Am. Chem. Soc.*, 2021, **143**, 18041–18051.
- 73 J. Xia, Z. Wang, N. D. Rodrig, B. Nan, J. Zhang, W. Zhang, B. L. Lucht, C. Yang and C. Wang, Super-reversible CuF<sub>2</sub> cathodes enabled by Cu<sup>2+</sup>-coordinated alginate, *Adv. Mater.*, 2022, **34**, 2205229.
- 74 C. Senthil, S.-S. Kim and H. Y. Jung, Flame retardant high-power Li-S flexible batteries enabled by bio-macromolecular binder integrating conformal fractions, *Nat. Commun.*, 2022, **13**, 145.
- 75 Z. Li, G. Wu, Y. Yang, Z. Wan, X. Zeng, L. Yan, S. Wu, M. Ling, C. Liang, K. N. Hui and Z. Lin, An ion-conductive grafted polymeric binder with practical loading for silicon anode with high interfacial stability in lithium-ion batteries, *Adv. Energy Mater.*, 2022, **12**, 2201197.
- 76 N. Xue, W. Wang, Z. Chen, Y. Heng, Z. Yuan, R. Xu and C. Lei, Electrochemically stable poly(vinylidene fluoride)-polyurethane polymer gel electrolytes with polar β-phase in lithium batteries, *J. Electroanal. Chem.*, 2022, **907**, 116026.
- 77 F. Chen, M.-x. Jing, H. Yang, W.-y. Yuan, M.-q. Liu, Y.-s. Ji, S. Hussain and X.-q. Shen, Improved ionic conductivity and Li dendrite suppression of PVDF-based solid electrolyte membrane by LLZO incorporation and mechanical reinforcement, *Ionics*, 2021, **27**, 1101–1111.
- 78 W. Yao, M. Chouchane, W. Li, S. Bai, Z. Liu, L. Li, A. X. Chen, B. Sayahpour, R. Shimizu, G. Raghavendran, M. A. Schroeder, Y.-T. Chen, D. H. S. Tan, B. Sreenarayanan, C. K. Waters, A. Sichler, B. Gould, D. J. Kountz, D. J. Lipomi, M. Zhang and Y. S. Meng, A 5 V-class cobalt-free battery cathode with high loading enabled by dry coating, *Energy Environ. Sci.*, 2023, **16**, 1620–1630.
- 79 J. Kim, J. Choi, K. Park, S. Kim, K. W. Nam, K. Char and J. W. Choi, Host-guest interlocked complex binder for silicon-graphite composite electrodes in lithium ion batteries, *Adv. Energy Mater.*, 2022, **12**, 2103718.
- 80 Y. Hu, D. Shao, Y. Chen, J. Peng, S. Dai, M. Huang, Z.-H. Guo, X. Luo and K. Yue, A physically cross-linked hydrogen-bonded polymeric composite binder for high-performance silicon anodes, *ACS Appl. Energy Mater.*, 2021, **4**, 10886–10895.
- 81 C. Wang, H. Wu, Z. Chen, M. T. McDowell, Y. Cui and Z. Bao, Self-healing chemistry enables the stable operation of silicon microparticle anodes for high-energy lithium-ion batteries, *Nat. Chem.*, 2013, **5**, 1042–1048.
- 82 Y. K. Jeong, T.-w. Kwon, I. Lee, T.-S. Kim, A. Coskun and J. W. Choi, Millipede-inspired structural design principle for high performance polysaccharide binders in silicon anodes, *Energy Environ. Sci.*, 2015, **8**, 1224–1230.
- 83 A. Strand, J. Kouko, A. Oksanen, K. Salminen, A. Ketola, E. Retulainen and A. Sundberg, Enhanced strength, stiffness and elongation potential of paper by spray addition of polysaccharides, *Cellulose*, 2019, **26**, 3473–3487.
- 84 H. Wang, J. Fu, C. Wang, R. Zhang, Y. Yang, Y. Li, C. Li, Q. Sun, H. Li and T. Zhai, A universal aqueous conductive binder for flexible electrodes, *Adv. Funct. Mater.*, 2021, **31**, 2102284.
- 85 H. Li, L. Peng, D. Wu, J. Wu, Y.-J. Zhu and X. Hu, Ultrahigh-capacity and fire-resistant LiFePO<sub>4</sub>-based composite cathodes for advanced lithium-ion batteries, *Adv. Energy Mater.*, 2019, **9**, 1802930.
- 86 Y. Li, Y. Wu, T. Ma, Z. Wang, Q. Gao, J. Xu, L. Chen, H. Li and F. Wu, Long-life sulfide all-solid-state battery enabled by substrate-modulated dry-process binder, *Adv. Energy Mater.*, 2022, **12**, 2201732.
- 87 T. Liu, Q. Chu, C. Yan, S. Zhang, Z. Lin and J. Lu, Interweaving 3D network binder for high-areal-capacity Si anode through combined hard and soft polymers, *Adv. Energy Mater.*, 2019, **9**, 1802645.
- 88 D. G. Mackanic, X. Yan, Q. Zhang, N. Matsuhisa, Z. Yu, Y. Jiang, T. Manika, J. Lopez, H. Yan, K. Liu, X. Chen, Y. Cui and Z. Bao, Decoupling of mechanical properties and ionic conductivity in supramolecular lithium ion conductors, *Nat. Commun.*, 2019, **10**, 5384.
- 89 T. Dong, H. Zhang, R. Hu, P. Mu, Z. Liu, X. Du, C. Lu, G. Lu, W. Liu and G. Cui, A rigid-flexible coupling poly(vinylene carbonate) based cross-linked network: A versatile polymer platform for solid-state polymer lithium batteries, *Energy Storage Mater.*, 2022, **50**, 525–532.



- 90 J. Park, N. Willenbacher and K. H. Ahn, How the interaction between styrene-butadiene-rubber (SBR) binder and a secondary fluid affects the rheology, microstructure and adhesive properties of capillary-suspension-type graphite slurries used for Li-ion battery anodes, *Colloids Surf., A*, 2019, **579**, 123692.
- 91 H. Isozumi, T. Horiba, K. Kubota, K. Hida, T. Matsuyama, S. Yasuno and S. Komaba, Application of modified styrene-butadiene-rubber-based latex binder to high-voltage operating LiCoO<sub>2</sub> composite electrodes for lithium-ion batteries, *J. Power Sources*, 2020, **468**, 228332.
- 92 G. M. Zhou, K. Liu, Y. C. Fan, M. Q. Yuan, B. F. Liu, W. Liu, F. F. Shi, Y. Y. Liu, W. Chen, J. Lopez, D. Zhuo, J. Zhao, Y. C. Tsao, X. Y. Huang, Q. F. Zhang and Y. Cui, An aqueous inorganic polymer binder for high performance lithium-sulfur batteries with flame-retardant properties, *ACS Cent. Sci.*, 2018, **4**, 260–267.
- 93 J.-Y. Eom and L. Cao, Effect of anode binders on low-temperature performance of automotive lithium-ion batteries, *J. Power Sources*, 2019, **441**, 227178.
- 94 W. Zeng, L. Wang, X. Peng, T. Liu, Y. Jiang, F. Qin, L. Hu, P. K. Chu, K. Huo and Y. Zhou, Enhanced ion conductivity in conducting polymer binder for high-performance silicon anodes in advanced lithium-ion batteries, *Adv. Energy Mater.*, 2018, **8**, 1702314.
- 95 C. Park, Y. H. Kim, H. Lee, H. S. Kang, T. Kim, S. W. Lee, K. Lee, K.-B. Kim and C. Park, Conductor-free anode of transition metal dichalcogenide nanosheets self-assembled with graft polymer Li-ion channels, *Adv. Energy Mater.*, 2021, **11**, 2003243.
- 96 J. Lee, K. Lee, T. Lee, H. Kim, K. Kim, W. Cho, A. Coskun, K. Char and J. W. Choi, In situ deprotection of polymeric binders for solution-processible sulfide-based all-solid-state batteries, *Adv. Mater.*, 2020, **32**, 2001702.
- 97 I. D. Seymour, E. Quérel, R. H. Brugge, F. M. Pesci and A. Agüero, Understanding and engineering interfacial adhesion in solid-state batteries with metallic anodes, *ChemSusChem*, 2023, **16**, e202202215.
- 98 G. Raos and B. Zappone, Polymer adhesion: Seeking new solutions for an old problem, *Macromolecules*, 2021, **54**, 10617–10644.
- 99 P. Mu, S. Zhang, H. Zhang, J. Li, Z. Liu, S. Dong and G. Cui, Spider-inspired hierarchical structure binder achieves highly integrated silicon-based electrodes, *Adv. Mater.*, 2023, 2303312.
- 100 L. Hu, M. Jin, Z. Zhang, H. Chen, F. B. Ajdari and J. Song, Interface-adaptive binder enabled by supramolecular interactions for high-capacity Si/C composite anodes in lithium-ion batteries, *Adv. Funct. Mater.*, 2022, **32**, 2111560.
- 101 Z. Z. Chen, M. J. Lu, Y. Qian, Y. Yang, J. Liu, Z. Lin, D. J. Yang, J. Lu and X. Q. Qiu, Ultra-low dosage lignin binder for practical lithium-sulfur batteries, *Adv. Energy Mater.*, 2023, **13**, 2300092.
- 102 Z. Song, T. Zhang, L. Wang, Y. Zhao, Z. Li, M. Zhang, K. Wang, S. Xue, J. Fang, Y. Ji, F. Pan and L. Yang, Bio-inspired binder design for a robust conductive network in silicon-based anodes, *Small Methods*, 2022, **6**, 2101591.
- 103 B. Jin, L. Yang, J. Zhang, Y. Cai, J. Zhu, J. Lu, Y. Hou, Q. He, H. Xing, X. Zhan, F. Chen and Q. Zhang, Bioinspired binders actively controlling ion migration and accommodating volume change in high sulfur loading lithium-sulfur batteries, *Adv. Energy Mater.*, 2019, **9**, 1902938.
- 104 S. Kim, Y. K. Jeong, Y. Wang, H. Lee and J. W. Choi, A “sticky” mucin-inspired DNA-polysaccharide binder for silicon and silicon-graphite blended anodes in lithium-ion batteries, *Adv. Mater.*, 2018, **30**, 1707594.
- 105 Y. Liu, Z. Tai, T. Zhou, V. Sencadas, J. Zhang, L. Zhang, K. Konstantinov, Z. Guo and H. K. Liu, An all-integrated anode via interlinked chemical bonding between double-shelled-yolk-structured silicon and binder for lithium-ion batteries, *Adv. Mater.*, 2017, **29**, 1703028.
- 106 J. X. Song, M. J. Zhou, R. Yi, T. Xu, M. L. Gordin, D. H. Tang, Z. X. Yu, M. Regula and D. H. Wang, Interpenetrated gel polymer binder for high-performance silicon anodes in lithium-ion batteries, *Adv. Funct. Mater.*, 2014, **24**, 5904–5910.
- 107 Z.-Y. Wu, L. Deng, J.-T. Li, Q.-S. Huang, Y.-Q. Lu, J. Liu, T. Zhang, L. Huang and S.-G. Sun, Multiple hydrogel alginate binders for Si anodes of lithium-ion battery, *Electrochim. Acta*, 2017, **245**, 371–378.
- 108 Z. H. Li, Z. W. Wan, X. Q. Zeng, S. M. Zhang, L. J. Yan, J. P. Ji, H. X. Wang, Q. X. Ma, T. F. Liu, Z. Lin, M. Ling and C. D. Liang, A robust network binder via localized linking by small molecules for high-areal-capacity silicon anodes in lithium-ion batteries, *Nano Energy*, 2021, **79**, 105430.
- 109 D. X. Cao, Q. Li, X. Sun, Y. Wang, X. H. Zhao, E. Cakmak, W. T. Liang, A. Anderson, S. Ozcan and H. L. Zhu, Amphipathic binder integrating ultrathin and highly ion-conductive sulfide membrane for cell-level high-energy-density all-solid-state batteries, *Adv. Mater.*, 2021, **33**, 2105505.
- 110 F. Klein, B. Jache, A. Bhide and P. Adelhelm, Conversion reactions for sodium-ion batteries, *Phys. Chem. Chem. Phys.*, 2013, **15**, 15876–15887.
- 111 H. Yuan, J. Q. Huang, H. J. Peng, M. M. Titirici, R. Xiang, R. J. Chen, Q. B. Liu and Q. Zhang, A review of functional binders in lithium-sulfur batteries, *Adv. Energy Mater.*, 2018, **8**, 1802107.
- 112 G. Bucci, B. Talamini, A. Renuka Balakrishna, Y.-M. Chiang and W. C. Carter, Mechanical instability of electrode-electrolyte interfaces in solid-state batteries, *Phys. Rev. Mater.*, 2018, **2**, 105407.
- 113 L. Yu, Q. Yang, G. Zhu and R. Che, Preparation of yolk-shell urchin-like porous Co<sub>3</sub>O<sub>4</sub>/NiO@C microspheres with excellent lithium storage performance, *Ind. Chem. Mater.*, 2023, **1**, 247–253.
- 114 B. Zhang, Y. Dong, J. Han, Y. Zhen, C. Hu and D. Liu, Physicochemical dual crosslinking conductive polymeric networks combining high strength and high toughness



- enable stable operation of silicon microparticles anodes, *Adv. Mater.*, 2023, **35**, 2301320.
- 115 F. Zeng, W. Wang, A. Wang, K. Yuan, Z. Jin and Y.-s. Yang, Multidimensional polycation beta-cyclodextrin polymer as an effective aqueous binder for high sulfur loading cathode in lithium-sulfur batteries, *ACS Appl. Mater. Interfaces*, 2015, **7**, 26257–26265.
- 116 J. Wang, Z. Yao, C. W. Monroe, J. Yang and Y. Nuli, Carbonyl-beta-cyclodextrin as a novel binder for sulfur composite cathodes in rechargeable lithium batteries, *Adv. Funct. Mater.*, 2013, **23**, 1194–1201.
- 117 Y. K. Jeong, T.-w. Kwon, I. Lee, T.-S. Kim, A. Coskun and J. W. Choi, Hyperbranched beta-cyclodextrin polymer as an effective multidimensional binder for silicon anodes in lithium rechargeable batteries, *Nano Lett.*, 2014, **14**, 864–870.
- 118 D.-J. Yoo, A. Elabd, S. Choi, Y. Cho, J. Kim, S. J. Lee, S. H. Choi, T.-w. Kwon, K. Char, K. J. Kim, A. Coskun and J. W. Choi, Highly elastic polyrotaxane binders for mechanically stable lithium hosts in lithium-metal batteries, *Adv. Mater.*, 2019, **31**, 1901645.
- 119 Y.-H. Lee, J. Min, K. Lee, S. Kim, S. H. Park and J. W. Choi, Low molecular weight spandex as a promising polymeric binder for LiFePO<sub>4</sub> electrodes, *Adv. Energy Mater.*, 2017, **7**, 1602147.
- 120 B. Chang, J. Kim, Y. Cho, I. Hwang, M. S. Jung, K. Char, K. T. Lee, K. J. Kim and J. W. Choi, Highly elastic binder for improved cyclability of nickel-rich layered cathode materials in lithium-ion batteries, *Adv. Energy Mater.*, 2020, **10**, 2001069.
- 121 T. Y. Kwon, K. T. Kim, D. Y. Oh, Y. B. Song, S. Jun and Y. S. Jung, Three-dimensional networking binders prepared in situ during wet-slurry process for all-solid-state batteries operating under low external pressure, *Energy Storage Mater.*, 2022, **49**, 219–226.
- 122 H. Chen, Z. Z. Wu, Z. Su, S. Chen, C. Yan, M. Al-Mamun, Y. B. Tang and S. Q. Zhang, A mechanically robust self-healing binder for silicon anode in lithium ion batteries, *Nano Energy*, 2021, **81**, 105654.
- 123 T. Munaoka, X. Yan, J. Lopez, J. W. F. To, J. Park, J. B. H. Tok, Y. Cui and Z. Bao, Ionically conductive self-healing binder for low cost Si microparticles anodes in Li-ion batteries, *Adv. Energy Mater.*, 2018, **8**, 1703138.
- 124 Z. Chen, C. Wang, J. Lopez, Z. Lu, Y. Cui and Z. Bao, High-areal-capacity silicon electrodes with low-cost silicon particles based on spatial control of self-healing binder, *Adv. Energy Mater.*, 2015, **5**, 1401826.
- 125 X. Jiao, J. Yin, X. Xu, J. Wang, Y. Liu, S. Xiong, Q. Zhang and J. Song, Highly energy-dissipative, fast self-healing binder for stable Si anode in lithium-ion batteries, *Adv. Funct. Mater.*, 2021, **31**, 2005699.
- 126 B. Jin, D. Wang, J. Zhu, H. Guo, Y. Hou, X. Gao, J. Lu, X. Zhan, X. He and Q. Zhang, A self-healable polyelectrolyte binder for highly stabilized sulfur, silicon, and silicon oxides electrodes, *Adv. Funct. Mater.*, 2021, **31**, 2104433.
- 127 H. A. Lee, M. Shin, J. Kim, J. W. Choi and H. Lee, Designing adaptive binders for microenvironment settings of silicon anode particles, *Adv. Mater.*, 2021, **33**, 2007460.
- 128 B. L. D. Rinkel, D. S. Hall, I. Temprano and C. P. Grey, Electrolyte oxidation pathways in lithium-ion batteries, *J. Am. Chem. Soc.*, 2020, **142**, 15058–15074.
- 129 T. T. Dong, H. R. Zhang, Y. Ma, J. J. Zhang, X. F. Du, C. L. Lu, X. H. Shangguan, J. D. Li, M. Zhang, J. F. Yang, X. H. Zhou and G. L. Cui, A well-designed water-soluble binder enlightening the 5 V-class LiNi<sub>0.5</sub>Mn<sub>1.5</sub>O<sub>4</sub> cathodes, *J. Mater. Chem. A*, 2019, **7**, 24594–24601.
- 130 B. Chang, D. H. Yun, I. Hwang, J. K. Seo, J. Kang, G. Noh, S. Choi and J. W. Choi, Carrageenan as a sacrificial binder for 5 V LiNi<sub>0.5</sub>Mn<sub>1.5</sub>O<sub>4</sub> cathodes in lithium-ion batteries, *Adv. Mater.*, 2023, 2303787.
- 131 S.-J. Zhang, Y.-P. Deng, Q.-H. Wu, Y. Zhou, J.-T. Li, Z.-Y. Wu, Z.-W. Yin, Y.-Q. Lu, C.-H. Shen, L. Huang and S.-G. Sun, Sodium- alginate-based binders for lithium-rich cathode materials in lithium-ion batteries to suppress voltage and capacity fading, *ChemElectroChem*, 2018, **5**, 1321–1329.
- 132 J. Li, C.-H. Chang and A. Manthiram, Toward long-life, ultrahigh-nickel layered oxide cathodes for lithium-ion batteries: Optimizing the interphase chemistry with a dual-functional polymer, *Chem. Mater.*, 2020, **32**, 759–768.
- 133 L. Han, T. F. Liu, O. W. Sheng, Y. J. Liu, Y. Wang, J. W. Nai, L. Zhang and X. Y. Tao, Undervalued roles of binder in modulating solid electrolyte interphase formation of silicon-based anode materials, *ACS Appl. Mater. Interfaces*, 2021, **13**, 45139–45148.
- 134 K. L. Browning, R. L. Sacchi, M. Doucet, J. F. Browning, J. R. Kim and G. M. Veith, The study of the binder poly(acrylic acid) and its role in concomitant solid–electrolyte interphase formation on Si anodes, *ACS Appl. Mater. Interfaces*, 2020, **12**, 10018–10030.
- 135 K. L. Browning, J. F. Browning, M. Doucet, N. L. Yamada, G. Liu and G. M. Veith, Role of conductive binder to direct solid– electrolyte interphase formation over silicon anodes, *Phys. Chem. Chem. Phys.*, 2019, **21**, 17356–17365.
- 136 A. Pradhan, R. Badam, R. Miyairi, N. Takamori and N. Matsumi, Extreme fast charging capability in graphite anode via a lithium borate type biobased polymer as aqueous polyelectrolyte binder, *ACS Mater. Lett.*, 2023, **5**, 413–420.
- 137 Y. Wang, X. Yang, Y. Yuan, Z. Wang, H. Zhang and X. Li, N-rich solid electrolyte interface constructed in situ via a binder strategy for highly stable silicon anode, *Adv. Funct. Mater.*, 2023, 2301716.
- 138 H. Zhao, Y. Wei, C. Wang, R. Qiao, W. Yang, P. B. Messersmith and G. Liu, Mussel-inspired conductive polymer binder for Si- alloy anode in lithium-ion batteries, *ACS Appl. Mater. Interfaces*, 2018, **10**, 5440–5446.
- 139 Y. Wang, Y. Shi, L. Pan, Y. Ding, Y. Zhao, Y. Li, Y. Shi and G. Yu, Dopant-enabled supramolecular approach for controlled synthesis of nanostructured conductive polymer hydrogels, *Nano Lett.*, 2015, **15**, 7736–7741.
- 140 D. Liu, Y. Zhao, R. Tan, L.-L. Tian, Y. Liu, H. Chen and F. Pan, Novel conductive binder for high-performance silicon





- anodes in lithium ion batteries, *Nano Energy*, 2017, **36**, 206–212.
- 141 G. Liu, S. Xun, N. Vukmirovic, X. Song, P. Olalde-Velasco, H. Zheng, V. S. Battaglia, L. Wang and W. Yang, Polymers with tailored electronic structure for high capacity lithium battery electrodes, *Adv. Mater.*, 2011, **23**, 4679–4683.
- 142 M. Y. Wu, X. C. Xiao, N. Vukmirovic, S. D. Xun, P. K. Das, X. Y. Song, P. Olalde-Velasco, D. D. Wang, A. Z. Weber, L. W. Wang, V. S. Battaglia, W. L. Yang and G. Liu, Toward an ideal polymer binder design for high-capacity battery anodes, *J. Am. Chem. Soc.*, 2013, **135**, 12048–12056.
- 143 G. Ai, Y. Dai, Y. Ye, W. Mao, Z. Wang, H. Zhao, Y. Chen, J. Zhu, Y. Fu, V. Battaglia, J. Guo, V. Srinivasan and G. Liu, Investigation of surface effects through the application of the functional binders in lithium sulfur batteries, *Nano Energy*, 2015, **16**, 28–37.
- 144 H. An, X. Li, C. Chalker, M. Stracke, R. Verduzco and J. L. Lutkenhaus, Conducting block copolymer binders for carbon-free hybrid vanadium pentoxide cathodes with enhanced performance, *ACS Appl. Mater. Interfaces*, 2016, **8**, 28585–28591.
- 145 A. E. Javier, S. N. Patel, D. T. Hallinan Jr, V. Srinivasan and N. P. Balsara, Simultaneous electronic and ionic conduction in a block copolymer: Application in lithium battery electrodes, *Angew. Chem., Int. Ed.*, 2011, **50**, 9848–9851.
- 146 H. An, J. Mike, K. A. Smith, L. Swank, Y.-H. Lin, S. L. Pesek, R. Verduzco and J. L. Lutkenhaus, Highly flexible self-assembled V<sub>2</sub>O<sub>5</sub> cathodes enabled by conducting diblock copolymers, *Sci. Rep.*, 2015, **5**, 14166.
- 147 N. Salem, M. Lavrisa and Y. Abu-Lebdeh, Ionically-functionalized poly(thiophene) conductive polymers as binders for silicon and graphite anodes for Li-ion batteries, *Energy Technol.*, 2016, **4**, 331–340.
- 148 T. M. Higgins, S.-H. Park, P. J. King, C. Zhang, N. McEvoy, N. C. Berner, D. Daly, A. Shmeliov, U. Khan, G. Duesberg, V. Nicolosi and J. N. Coleman, A commercial conducting polymer as both binder and conductive additive for silicon nanoparticle-based lithium-ion battery negative electrodes, *ACS Nano*, 2016, **10**, 3702–3713.
- 149 T. Liu, C.-J. Tong, B. Wang, L.-M. Liu, S. Zhang, Z. Lin, D. Wang and J. Lu, Trifunctional electrode additive for high active material content and volumetric lithium-ion electrode densities, *Adv. Energy Mater.*, 2019, **9**, 1803390.
- 150 H. Wu, G. Yu, L. Pan, N. Liu, M. T. McDowell, Z. Bao and Y. Cui, Stable Li-ion battery anodes by in-situ polymerization of conducting hydrogel to conformally coat silicon nanoparticles, *Nat. Commun.*, 2013, **4**, 1943.
- 151 Y. Shi, J. Zhang, A. M. Bruck, Y. Zhang, J. Li, E. A. Stach, K. J. Takeuchi, A. C. Marschilok, E. S. Takeuchi and G. Yu, A tunable 3D nanostructured conductive gel framework electrode for high-performance lithium ion batteries, *Adv. Mater.*, 2017, **29**, 1603922.
- 152 B. Liu, P. Soares, C. Checkles, Y. Zhao and G. Yu, Three-dimensional hierarchical ternary nanostructures for high-performance Li-ion battery anodes, *Nano Lett.*, 2013, **13**, 3414–3419.
- 153 S.-J. Park, H. Zhao, G. Ai, C. Wang, X. Song, N. Yuca, V. S. Battaglia, W. Yang and G. Liu, Side-chain conducting and phase-separated polymeric binders for high-performance silicon anodes in lithium-ion batteries, *J. Am. Chem. Soc.*, 2015, **137**, 2565–2571.
- 154 P. Sengodu and A. D. Deshmukh, Conducting polymers and their inorganic composites for advanced Li-ion batteries: A review, *RSC Adv.*, 2015, **5**, 42109–42130.
- 155 D. Y. Oh, K. T. Kim, S. H. Jung, D. H. Kim, S. Jun, S. Jeoung, H. R. Moon and Y. S. Jung, Tactical hybrids of Li<sup>+</sup>-conductive dry polymer electrolytes with sulfide solid electrolytes: Toward practical all-solid-state batteries with wider temperature operability, *Mater. Today*, 2022, **53**, 7–15.
- 156 D. Y. Oh, Y. J. Nam, K. H. Park, S. H. Jung, K. T. Kim, A. R. Ha and Y. S. Jung, Slurry-fabricable Li<sup>+</sup>-conductive polymeric binders for practical all-solid-state lithium-ion batteries enabled by solvate ionic liquids, *Adv. Energy Mater.*, 2019, **9**, 1802927.
- 157 J. Gao, C. Wang, D.-W. Han and D.-M. Shin, Single-ion conducting polymer electrolytes as a key jigsaw piece for next-generation battery applications, *Chem. Sci.*, 2021, **12**, 13248–13272.
- 158 L. Li, T. A. Pascal, J. G. Connell, F. Y. Fan, S. M. Meckler, L. Ma, Y.-M. Chiang, D. Prendergast and B. A. Helms, Molecular understanding of polyelectrolyte binders that actively regulate ion transport in sulfur cathodes, *Nat. Commun.*, 2017, **8**, 2277.
- 159 S. B. Hong, Y. J. Lee, U. H. Kim, C. Bak, Y. M. Lee, W. Cho, H. J. Hah, Y. K. Sun and D. W. Kim, All-solid-state lithium batteries: Li<sup>+</sup>-conducting ionomer binder for dry-processed composite cathodes, *ACS Energy Lett.*, 2022, **7**, 1092–1100.
- 160 S. Jiang, B. Hu, Z. Shi, W. Chen, Z. Zhang and L. Zhang, Re-engineering poly(acrylic acid) binder toward optimized electrochemical performance for silicon lithium-ion batteries: Branching architecture leads to balanced properties of polymeric binders, *Adv. Funct. Mater.*, 2020, **30**, 1908558.
- 161 X. Wan, C. Kang, T. Mu, J. Zhu, P. Zuo, C. Du and G. Yin, A multilevel buffered binder network for high-performance silicon anodes, *ACS Energy Lett.*, 2022, **7**, 3572–3580.
- 162 D. O. Shin, H. Kim, J. Choi, M. P. Kim, J. Y. Kim, S. H. Kang, Y. S. Park, S. Y. Hong, M. Cho, Y. G. Lee, K. Y. J. Cho and Y. M. Lee, Electrolyte-free graphite electrode with enhanced interfacial conduction using Li<sup>+</sup>-conductive binder for high-performance all-solid-state batteries, *Energy Storage Mater.*, 2022, **49**, 481–492.
- 163 D. O. Shin, H. Kim, J. Choi, J. Y. Kim, S. H. Kang, Y.-S. Park, M. Cho, Y. M. Lee, K. Cho and Y.-G. Lee, Effect of Lithium Substitution Ratio of Polymeric Binders on Interfacial Conduction within All-Solid-State Battery Anodes, *ACS Appl. Mater. Interfaces*, 2023, **15**, 13131–13143.
- 164 Y. Wang, N. Dong, B. Liu, K. Qi, G. Tian, S. Qi and D. Wu, Enhanced electrochemical performance of the LiNi<sub>0.8</sub>Co<sub>0.1</sub>Mn<sub>0.1</sub>O<sub>2</sub> cathode via in-situ nanoscale surface modification with poly(imide-siloxane) binder, *Chem. Eng. J.*, 2022, **450**, 137959.



- 165 A. Ramgobin, G. Fontaine and S. Bourbigot, Thermal degradation and fire behavior of high performance polymers, *Polym. Rev.*, 2019, **59**, 55–123.
- 166 F. Safdari, P. J. Carreau, M. C. Heuzey, M. R. Kamal and M. M. Sain, Enhanced properties of poly(ethylene oxide)/cellulose nanofiber biocomposites, *Cellulose*, 2017, **24**, 755–767.
- 167 D. A. Gribble, Z. Li, B. Ozdogru, E. McCulfor, O. O. Capraz and V. G. Pol, Mechanistic elucidation of electronically conductive PEDOT:PSS tailored binder for a potassium-ion battery graphite anode: Electrochemical, mechanical, and thermal safety aspects, *Adv. Energy Mater.*, 2022, **12**, 2103439.
- 168 H. Q. Pham, J. Lee, H. M. Jung and S.-W. Song, Non-flammable  $\text{LiNi}_{0.8}\text{Co}_{0.1}\text{Mn}_{0.1}\text{O}_2$  cathode via functional binder; stabilizing high-voltage interface and performance for safer and high-energy lithium rechargeable batteries, *Electrochim. Acta*, 2019, **317**, 711–721.
- 169 G. Qian, L. Wang, Y. Shang, X. He, S. Tang, M. Liu, T. Li, G. Zhang and J. Wang, Polyimide binder: A facile way to improve safety of lithium ion batteries, *Electrochim. Acta*, 2016, **187**, 113–118.
- 170 M. Monisha, P. Permude, A. Ghosh, A. Kumar, S. Zafar, S. Mitra and B. Lochab, Halogen-free flame-retardant sulfur copolymers with stable Li-S battery performance, *Energy Storage Mater.*, 2020, **29**, 350–360.
- 171 M. Liu, P. Chen, X. Pan, S. Pan, X. Zhang, Y. Zhou, M. Bi, J. Sun, S. Yang, A. L. Vasiliev, P. J. Kulesza, X. Ouyang, J. Xu, X. Wang, J. Zhu and Y. Fu, Synergism of flame-retardant, self-healing, high-conductive and polar to a multi-functional binder for lithium-sulfur batteries, *Adv. Funct. Mater.*, 2022, **32**, 2205031.
- 172 K. Chen, S. Shinjo, A. Sakuda, K. Yamamoto, T. Uchiyama, K. Kuratani, T. Takeuchi, Y. Orikasa, A. Hayashi, M. Tatsumisago, Y. Kimura, T. Nakamura, K. Amezawa and Y. Uchimoto, Morphological effect on reaction distribution influenced by binder materials in composite electrodes for sheet-type all-solid-state lithium-ion batteries with the sulfide-based solid electrolyte, *J. Phys. Chem. C*, 2019, **123**, 3292–3298.
- 173 K. T. Kim, D. Y. Oh, S. Jun, Y. B. Song, T. Y. Kwon, Y. Han and Y. S. Jung, Tailoring slurries using cosolvents and Li salt targeting practical all-solid-state batteries employing sulfide solid electrolytes, *Adv. Energy Mater.*, 2021, **11**, 2003766.
- 174 J. M. Kim, Y. Cho, V. Guccini, M. Hahn, B. Y. Yan, G. Salazar-Alvarez and Y. Piao, TEMPO-oxidized cellulose nanofibers as versatile additives for highly stable silicon anode in lithium-ion batteries, *Electrochim. Acta*, 2021, **369**, 137708.
- 175 S. Jaiser, J. Kumberg, J. Klaver, J. L. Urai, W. Schabel, J. Schmatz and P. Scharfer, Microstructure formation of lithium-ion battery electrodes during drying – An ex-situ study using cryogenic broad ion beam slope-cutting and scanning electron microscopy (Cryo-BIB-SEM), *J. Power Sources*, 2017, **345**, 97–107.
- 176 A. Bielefeld, D. A. Weber and J. Janek, Modeling effective ionic conductivity and binder influence in composite cathodes for all-solid-state batteries, *ACS Appl. Mater. Interfaces*, 2020, **12**, 12821–12833.
- 177 C. Guo, M. Liu, G.-K. Gao, X. Tian, J. Zhou, L.-Z. Dong, Q. Li, Y. Chen, S.-L. Li and Y.-Q. Lan, Anthraquinone covalent organic framework hollow tubes as binder microadditives in Li-S batteries, *Angew. Chem., Int. Ed.*, 2022, **61**, e202113315.
- 178 M. Ryu, Y.-K. Hong, S.-Y. Lee and J. H. Park, Ultrahigh loading dry-process for solvent-free lithium-ion battery electrode fabrication, *Nat. Commun.*, 2023, **14**, 1316.
- 179 D. Bresser, D. Buchholz, A. Moretti, A. Varzi and S. Passerini, Alternative binders for sustainable electrochemical energy storage - the transition to aqueous electrode processing and bio-derived polymers, *Energy Environ. Sci.*, 2018, **11**, 3096–3127.
- 180 G. Li, M. Ling, Y. Ye, Z. Li, J. Guo, Y. Yao, J. Zhu, Z. Lin and S. Zhang, Acacia senegal-inspired bifunctional binder for longevity of lithium-sulfur batteries, *Adv. Energy Mater.*, 2015, **5**, 1500878.
- 181 O. S. Taskin, D. Hubble, T. Zhu and G. Liu, Biomass-derived polymeric binders in silicon anodes for battery energy storage applications, *Green Chem.*, 2021, **23**, 7890–7901.
- 182 L. Jing, Y. Ji, L. Feng, X. Fu, X. He, Y. He, Z. Zhu, X. Sun, Z. Liu, M. Yang, W. Yang and Y. Wang, Faster and better: A polymeric chaperone binder for microenvironment management in thick battery electrodes, *Energy Storage Mater.*, 2022, **45**, 828–839.
- 183 Y. Zou, J. Cao, H. Li, W. Wu, Y. Liang and J. Zhang, Large-scale direct regeneration of  $\text{LiFePO}_4@C$  based on spray drying, *Ind. Chem. Mater.*, 2023, **1**, 254–261.
- 184 J. Ahn, H.-G. Im, Y. Lee, D. Lee, H. Jang, Y. Oh, K. Chung, T. Park, M.-K. Um, J. W. Yi, J. Kim, D. J. Kang and J.-K. Yoo, A novel organosilicon-type binder for  $\text{LiCoO}_2$  cathode in Li-ion batteries, *Energy Storage Mater.*, 2022, **49**, 58–66.
- 185 M. Ling, J. Qiu, S. Li, C. Yan, M. J. Kiefel, G. Liu and S. Zhang, Multifunctional SA-PPRODOT binder for lithium ion batteries, *Nano Lett.*, 2015, **15**, 4440–4447.
- 186 Y. Ma, K. Chen, J. Ma, G. Xu, S. Dong, B. Chen, J. Li, Z. Chen, X. Zhou and G. Cui, A biomass based free radical scavenger binder endowing a compatible cathode interface for 5 V lithium-ion batteries, *Energy Environ. Sci.*, 2019, **12**, 273–280.
- 187 L. Hu, X. Zhang, P. Zhao, H. Fan, Z. Zhang, J. Deng, G. Ungar and J. Song, Gradient H-bonding binder enables stable high-areal-capacity Si-based anodes in pouch cells, *Adv. Mater.*, 2021, **33**, 2104416.
- 188 S. L. Chou, Y. D. Pan, J. Z. Wang, H. K. Liu and S. X. Dou, Small things make a big difference: Binder effects on the performance of Li and Na batteries, *Phys. Chem. Chem. Phys.*, 2014, **16**, 20347–20359.
- 189 Y. Shi, X. Y. Zhou and G. H. Yu, Material and structural design of novel binder systems for high-energy, high-power lithium-ion batteries, *Acc. Chem. Res.*, 2017, **50**, 2642–2652.



- 190 S. Chen, Z. Song, L. Wang, H. Chen, S. Zhang, F. Pan and L. Yang, Establishing a resilient conductive binding network for Si- based anodes via molecular engineering, *Acc. Chem. Res.*, 2022, **55**, 2088–2102.
- 191 Y. M. Zhao, F. S. Yue, S. C. Li, Y. Zhang, Z. R. Tian, Q. Xu, S. Xin and Y. G. Guo, Advances of polymer binders for silicon-based anodes in high energy density lithium-ion batteries, *InfoMat*, 2021, **3**, 460–501.
- 192 L. C. Gallegos, G. Luchini, P. C. St. John, S. Kim and R. S. Paton, Importance of engineered and learned molecular representations in predicting organic reactivity, selectivity, and chemical properties, *Acc. Chem. Res.*, 2021, **54**, 827–836.
- 193 J. P. Reid and M. S. Sigman, Holistic prediction of enantioselectivity in asymmetric catalysis, *Nature*, 2019, **571**, 343–348.
- 194 L.-C. Xu, J. Frey, X. Hou, S.-Q. Zhang, Y.-Y. Li, J. C. A. Oliveira, S.-W. Li, L. Ackermann and X. Hong, Enantioselectivity prediction of pallada-electrocatalysed C–H activation using transition state knowledge in machine learning, *Nat. Synth.*, 2023, **2**, 321–330.
- 195 A. F. Zahrt, J. J. Henle, B. T. Rose, Y. Wang, W. T. Darrow and S. E. Denmark, Prediction of higher-selectivity catalysts by computer-driven workflow and machine learning, *Science*, 2019, **363**, eaau5631.
- 196 J. H. Lee, J. Kim, M. H. Jeong, K. H. Ahn, H. L. Lee and H. J. Youn, Visualization of styrene-butadiene rubber (SBR) latex and large-scale analysis of the microstructure of lithium-ion battery (LIB) anodes, *J. Power Sources*, 2023, **557**, 232552.
- 197 S. Mueller, M. Lippuner, M. Verezhak, V. De Andrade, F. De Carlo and V. Wood, Multimodal nanoscale tomographic imaging for battery electrodes, *Adv. Energy Mater.*, 2020, **10**, 1904119.
- 198 T.-T. Nguyen, J. Villanova, Z. Su, R. Tucoulou, B. Fleutot, B. Delobel, C. Delacourt and A. Demortiere, 3D quantification of microstructural properties of  $\text{LiNi}_{0.5}\text{Mn}_{0.3}\text{Co}_{0.2}\text{O}_2$  high energy density electrodes by X-ray holographic nanotomography, *Adv. Energy Mater.*, 2021, **11**, 2003529.
- 199 Y. S. Zhang, A. N. P. Radhakrishnan, J. B. Robinson, R. E. Owen, T. G. Tranter, E. Kendrick, P. R. Shearing and D. J. L. Brett, In situ ultrasound acoustic measurement of the lithium-ion battery electrode drying process, *ACS Appl. Mater. Interfaces*, 2021, **13**, 36605–36620.
- 200 N. Shpigel, M. D. Levi, S. Sigalov, O. Girshevitz, D. Aurbach, L. Daikhin, N. Jaekel and V. Presser, Non-invasive in situ dynamic monitoring of elastic properties of composite battery electrodes by EQCM-D, *Angew. Chem., Int. Ed.*, 2015, **54**, 12353–12356.
- 201 H. Hagiwara, W. J. Suszynski and L. F. Francis, A Raman spectroscopic method to find binder distribution in electrodes during drying, *J. Coat. Technol. Res.*, 2014, **11**, 11–17.
- 202 J. Xiong, N. Dupre, P. Moreau and B. Lestriez, From the direct observation of a PAA-based binder using STEM-VEELS to the ageing mechanism of silicon/graphite anode with high areal capacity cycled in an FEC-rich and EC-free electrolyte, *Adv. Energy Mater.*, 2022, **12**, 2103348.
- 203 S. Mueller, P. Pietsch, B.-E. Brandt, P. Baade, V. De Andrade, F. De Carlo and V. Wood, Quantification and modeling of mechanical degradation in lithium-ion batteries based on nanoscale imaging, *Nat. Commun.*, 2018, **9**, 2340.
- 204 T. Lombardo, A. C. Ngandjong, A. Belhcen and A. A. Franco, Carbon-binder migration: A three-dimensional drying model for lithium-ion battery electrodes, *Energy Storage Mater.*, 2021, **43**, 337–347.
- 205 Y. Li, Y. Wu, Z. Wang, J. Xu, T. Ma, L. Chen, H. Li and F. Wu, Progress in solvent-free dry-film technology for batteries and supercapacitors, *Mater. Today*, 2022, **55**, 92–109.
- 206 F. Hippauf, B. Schumm, S. Doerfler, H. Althues, S. Fujiki, T. Shiratsuchi, T. Tsujimura, Y. Aihara and S. Kaskel, Overcoming binder imitations of sheet-type solid-state cathodes using a solvent-free dry-film approach, *Energy Storage Mater.*, 2019, **21**, 390–398.

